# REPORT DOCUMENTATION PAGE

*Form Approved*
*OMB No. 0704-0188*



| 1. REPORT DATE *(DD-MM-YYYY)* | 2. REPORT TYPE | 3. DATES COVERED *(From 01-12-2008 To 30-11-2011)* |
|---|---|---|
| 07-08-2012 | Final Report | |

**4. TITLE AND SUBTITLE**
~~In~~vestigation of subgrid-scale mixing and turbulence-chemistry interaction in turbulent partially premixed flames

**5a. CONTRACT NUMBER**

**5b. GRANT NUMBER**
F-9550-09-1-0045

**5c. PROGRAM ELEMENT NUMBER**
61102F

**6. AUTHOR(S)**
Chenning Tong

**5d. PROJECT NUMBER**
2308

**5e. TASK NUMBER**
BX

**5f. WORK UNIT NUMBER**

**7. PERFORMING ORGANIZATION NAME(S) AND ADDRESS(ES)**

Department of Mechanical Engineering
Clemson University
Clemson, SC 29634

**8. PERFORMING ORGANIZATION REPORT NUMBER**

**9. SPONSORING / MONITORING AGENCY NAME(S) AND ADDRESS(ES)**
AFOSR/NA
875 Randolph Street
Suite 325, Room 3112
Arlington, VA 22203

**10. SPONSOR/MONITOR'S ACRONYM(S)**

**11. SPONSOR/MONITOR'S REPORT NUMBER(S)**
AFRL-OSR-VA-TR-2012-0959

**12. DISTRIBUTION / AVAILABILITY STATEMENT**

Approved for public release, distribution unlimited

**13. SUPPLEMENTARY NOTES**

**14. ABSTRACT**

This research project focused on issues met in using large-eddy simulation (LES) to predict turbulent nonpremixed/partially premixed combustion. In LES of such flames the subgrid-scale (SGS) scalar mixing and the resulting subgrid-scale scalar distributions must be faithfully represented. In this research the mixture fraction filtered mass density function (FMDF) of mixture fraction, temperature, and species mass fractions, the conditionally filtered dissipation rates and the conditionally filtered diffusion were studied experimentally using data from Sandia flames. The results show that the subgrid-scale mixture fraction has two limiting mixing regimes, which have strong effects on the flame structure. For the well mixed regimes the scalar diffusion had a simple structure whereas for the poorly mixed regime the diffusion structure was more complex, with the reaction and the spatial structure playing important roles. The results in the present study suggest that it is important for combustion models to predict accurately both distributed reaction zones and flamelets. Specifically, mixing models need to be able to account for the different SGS mixing structures.

**15. SUBJECT TERMS**

| 16. SECURITY CLASSIFICATION OF: | | | 17. LIMITATION OF ABSTRACT | 18. NUMBER OF PAGES | 19a. NAME OF RESPONSIBLE PERSON |
|---|---|---|---|---|---|
| a. REPORT | b. ABSTRACT | c. THIS PAGE | | | Chiping Li |
| Unclassified | Unclassified | Unclassified | UL | 39 | 19b. TELEPHONE NUMBER *(include area code)* 703 696-8478 |

# Final Report: Investigation of subgrid-scale mixing and turbulence-chemistry interaction in turbulent partially premixed flames

AFOSR Grant FA9550-09-1-0045

Principal Investigator: Chenning Tong

Department of Mechanical Engineering
Clemson University
Clemson, SC 29634-0921

## I Introduction

This research project focused on issues met in using large-eddy simulation (LES) to predict turbulent nonpremixed combustion. LES has been recognized as a very promising approach to model such flames[1, 2, 3]. In this approach the subgrid-scale (SGS) scalar mixing and the resulting instantaneous distribution of scalar values in each grid volume (i.e., the filtered density function) must be represented faithfully in order to predict accurately the chemical reaction rate. This research studied issues in using this LES approach by investigating the SGS mixing of the mixture fraction, the temperature, and the species mass fractions in turbulent partially premixed (Sandia) flames using experimental data. The first is a conserved scalar, whereas the latter ones are reactive scalars; therefore, the present study provides the physics for developing mixing models to treat SGS mixing of both conserved and reactive scalars. Specifically, the following work was completed:

- Investigated the filtered mass density function (FMDF) of the mixture fraction, the temperature, and the species mass fractions using experimental data. The FMDF and the structure of the SGS scalar were found to depend strongly on the SGS variance (degree of nonequilibrium spectral transfer).
- Investigated the conditionally filtered scalar dissipation rate, the conditionally filtered temperature dissipation rate, and the conditionally filtered species mass fraction dissipation rate conditional on the mixture fraction, the temperature, and the species mass fractions, which

are the most SGS important terms in the transport equation of the FMDF of the mixture fraction, the temperature, and the species mass fractions. The effects of the SGS mixture fraction structure on the SGS flame structure were studied.

- Investigated the conditionally filtered scalar diffusion, the conditionally filtered temperature diffusion, and the conditionally filtered species mass fraction diffusion conditional on the mixture fraction, the temperature, and the species mass fractions, which are the alternative forms of the SGS mixing terms in the transport equation of the FMDF of the mixture fraction, the temperature, and the species mass fractions.
- Further developed and tested a conditional sampling-based method for noise and resolution corrections for scalar dissipation rate measurements. Applied the method to turbulent partially premixed flames. This method is the first to make use of the unique property of the turbulent scalar fields, allowing high accuracy corrections even for highly noisy signals.

The primarily findings of this research are discussed in the following.

# II Nomenclature

| | |
|---|---|
| $\xi$ | mixture fraction |
| $\hat{\xi}$ | sample-space variable for mixture fraction |
| $T$ | temperature |
| $\hat{T}$ | sample-space variable for temperature |
| $Y_i$ | species mass fraction |
| $\hat{Y}_i$ | sample-space variable for species mass fraction |
| $\rho$ | mixture density |
| $F_{\xi L}(\hat{\xi}; \mathbf{x}, t)$ | mixture fraction filtered mass density function (FMDF) |
| $\chi$ | scalar dissipation rate |
| $\chi_T$ | temperature dissipation rate |
| $D$ | molecular diffusivity or jet diameter |

| | |
|---|---|
| $F_{\xi T Y_i L}(\hat{\xi}, \hat{T}, \hat{Y}_i; \mathbf{x}, t)$ | FMDF of mixture fraction, temperature, and species mass fraction |
| $\langle \xi \rangle_L$ | Favre filtered mixture fraction |
| $\langle \xi''^2 \rangle_L$ | Favre subgrid-scale scalar variance |
| $G(\mathbf{x})$ | filter function |
| $\Delta$ | filter size |
| $\langle \cdot \rangle_\ell$ | conventional filtered variable |
| $\langle \cdot \rangle_L$ | Favre filtered variable |
| $s$ | reaction rate for temperature |
| $n$ | measurement noise |
| $h$ | sample spacing |
| $C_N$ | scheme dependent coefficient in noise estimation |

# III Findings

The mixture fraction FMDF is defined as

$$F_{\xi L}(\hat{\xi}; \mathbf{x}, t) = \langle \rho(\mathbf{x}, t) \delta(\xi - \hat{\xi}; \mathbf{x}, t) \rangle_\ell = \int \rho(\mathbf{x}', t) \delta(\xi - \hat{\xi}; \mathbf{x}', t) G(\mathbf{x} - \mathbf{x}') d\mathbf{x}', \quad (1)$$

The FMDF transport equation is

$$\frac{\partial F_{\xi L}}{\partial t} + \frac{\partial}{\partial x_j} \{ \langle u_j | \hat{\xi} \rangle_L F_{\xi L} \} = \frac{\partial}{\partial x_j} (D \frac{\partial F_{\xi L}}{\partial x_j}) - \frac{\partial^2}{\partial \hat{\xi}^2} \{ \langle \chi | \hat{\xi} \rangle_L F_{\xi L} \}, \quad (2)$$

where $\chi = \langle 2D \frac{\partial \xi}{\partial x_j} \frac{\partial \xi}{\partial x_j} | \xi \rangle_\ell$ and $D$ are the scalar dissipation rate and the molecular diffusivity, respectively.

The filtered mass density function function of mixture fraction, temperature, and species mass fraction is

$$F_{\xi TY_i}(\hat{\xi},\hat{T},\hat{Y}_i;\mathbf{x},t) = \langle \rho(\mathbf{x},t)\delta(\xi-\hat{\xi})\delta(T-\hat{T})\delta(Y_i-\hat{Y}_i)\rangle_\ell = \int \rho(\mathbf{x}',t)\delta(\xi-\hat{\xi})\delta(T-\hat{T})\delta(Y_i-\hat{Y}_i)G(\mathbf{x}-\mathbf{x}')d\mathbf{x}', \quad (3)$$

The FMDF transport equation is

$$\frac{\partial F_{\phi L}}{\partial t} + \frac{\partial}{\partial x_j}\{\langle u_j|\hat{\boldsymbol{\phi}}\rangle_\ell F_{\phi L}\} = -\frac{\partial}{\partial \hat{\phi}_\alpha}\{\frac{1}{\rho(\hat{\boldsymbol{\phi}})}\langle\frac{\partial}{\partial x_j}(\rho D^{(\alpha)}\frac{\partial \phi_\alpha}{\partial x_j})|\hat{\boldsymbol{\phi}}\rangle_\ell F_{\phi L}\} - \frac{\partial}{\partial \hat{\phi}_\alpha}\{s_\alpha(\hat{\boldsymbol{\phi}})F_{\phi L}\}$$
$$= -\frac{\partial^2}{\partial x_j \hat{\phi}_\alpha}\{\langle D^{(\alpha)}\frac{\partial \phi_\alpha}{\partial x_j}|\hat{\boldsymbol{\phi}}\rangle_\ell F_{\phi L}\} - \frac{\partial^2}{\partial \hat{\phi}_\alpha \hat{\phi}_\beta}\{\langle D^{(\alpha)}\frac{\partial \phi_\alpha}{\partial x_j}\frac{\partial \phi_\beta}{\partial x_j}|\hat{\boldsymbol{\phi}}\rangle_\ell F_{\phi L}\} - \frac{\partial}{\partial \hat{\phi}_\alpha}\{s_\alpha(\hat{\boldsymbol{\phi}})F_{\phi L}\}, \quad (4)$$

where $D^{(\alpha)}$ (no summation for the superscript $\alpha$) is the molecular diffusivity. The reaction rate, $\mathbf{s}$, is a function of the species mass fractions and temperature $\boldsymbol{\phi}$; $\hat{\boldsymbol{\phi}}$ represents the sample-space variables for $\boldsymbol{\phi}$. The first two terms in the equation are the time rate of change and advection in physical space respectively. The rest of the terms include diffusion of the FMDF in physical space, transport of the FMDF in scalar space by the conditionally filtered mixture fraction diffusion, the conditionally filtered temperature diffusion, the conditionally filtered mixed dissipation, the conditionally filtered mixture fraction dissipation, the conditionally filtered temperature dissipation, and the reaction.

In this research we focused on the FMDF, the mixture fraction dissipation, and the temperature dissipation rate to investigate SGS mixing and turbulence-chemistry interaction. We used experimental data obtained in piloted turbulent partially premixed methane flames with a 1:3 ratio of $CH_4$ to air by volume (Sandia flames D and E, see Ref.[4, 5, 6]). The measurements employed combined line-imaging of Raman scattering, Rayleigh scattering, and laser-induced CO fluorescence. Simultaneous measurements of major species ($CO_2$, $O_2$, CO, $N_2$, $CH_4$, $H_2O$, and $H_2$), mixture fraction (obtained from all major species), temperature, and the radial component of scalar dissipation rate were made. The mixture fraction was calculated using a variation of Bilger's definition[7], which had been modified by excluding the oxygen terms[4]. In the following we briefly outline the results from our study and their implications for LES.

### A. Filtered mass density function of mixture fraction, temperature, and species mass fractions in turbulent partially premixed flames

The FMDF of $\xi$, $T$ and $Y_{CO_2}$ appears to be largely limited to a two-dimensional manifold and has a similar shape to the FMDF of $\xi$ and $T$ due to the strong correlation between $T$ and $Y_{CO_2}$ (Figs. 1 and 2), since the latter is directly related to the heat release. Consequently, although there

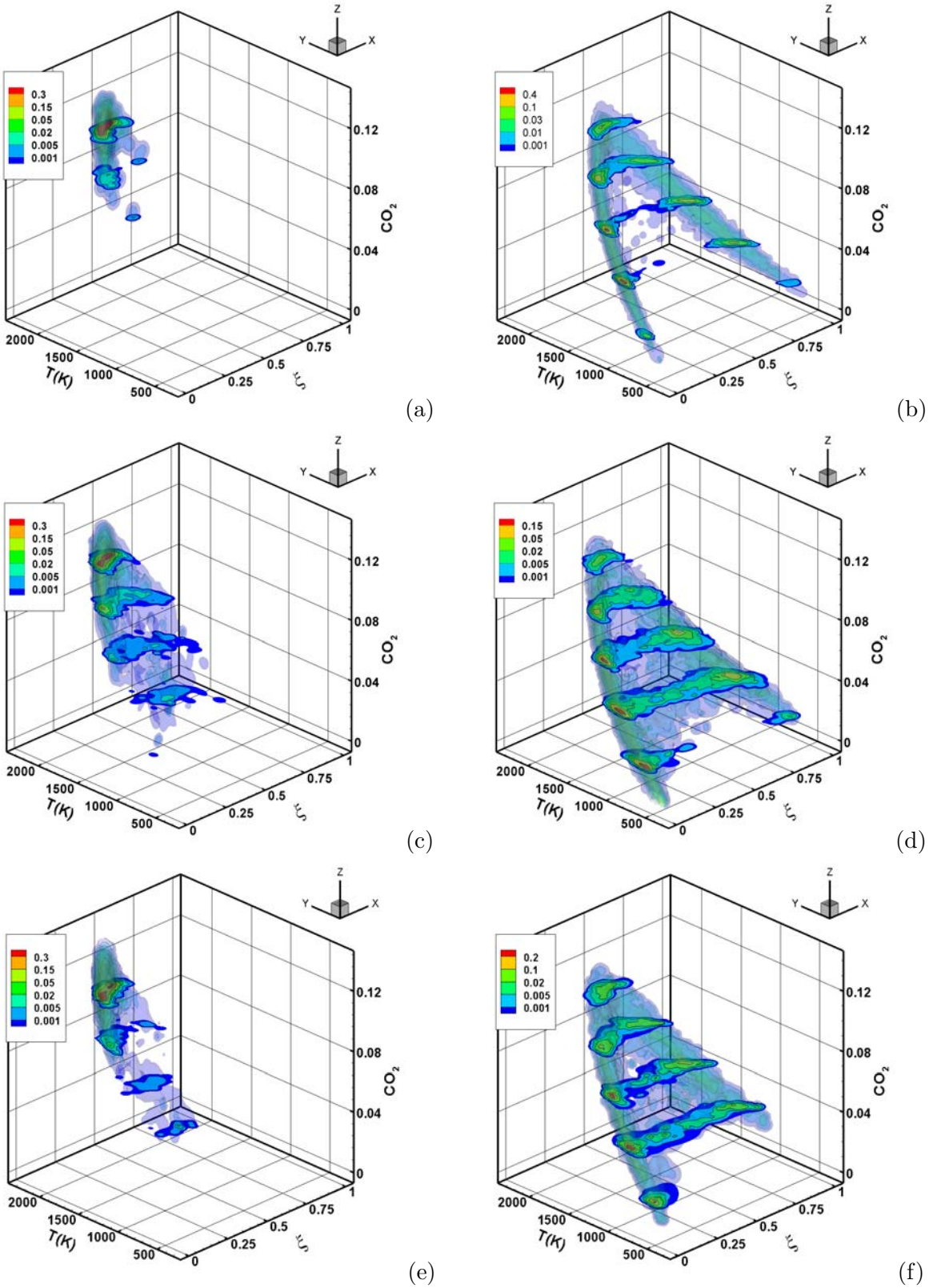


Figure 1: FMDF for $\xi$, $T$ and $Y_{CO_2}$ at $x/D = 7.5$, 15 and 30 in flame D, respectively. (ace) small SGS variance ($\langle\xi''^2\rangle_L = 0.0013$, $\langle\langle\xi''^2\rangle_L\rangle = 0.0272$). The color isosurfaces and contours denote the FMDF values; (bdf) large SGS variance ($\langle\xi''^2\rangle_L = 0.066$).

are four scalars in the mixing problem, i.e., $\xi$, $T$, $Y_{CO_2}$, and the co-flow, the SGS mixing is similar to three-scalar SGS mixing. Thus, the mixing problem for these scalars is a degenerated case. At $x/D = 7.5$ the flame is close to fully burning, with $T$ and $Y_{CO_2}$ not far from the equilibrium values. For small SGS variance, the FMDF is unimodal and is concentrated near the peak $T$ and $Y_{CO_2}$ (Fig. 1a). There are only a small number of extinguished samples. For large SGS variance, the FMDF is bimodal (Fig. 1b), indicating that the rich and lean mixtures in the SGS field (i.e., a grid cell) are essentially segregated. The SGS scalar contains two relatively well-mixed mixtures corresponding to the two peaks of the FMDF. The difference between the $\xi$ values of the two mixtures is greater than the reaction zone width in the $\xi$ space, $\Delta\xi_R$ ($\approx 0.23$), for the Sandia flames. Such a mixture fraction structure limits the reaction zones to thin diffusion layers, thereby resulting in laminar flamelets. For flame E both $T$ and $Y_{CO_2}$ are lower than those for flame D (not shown), and there is a relatively large probability of local extinction due to the higher scalar dissipation rate, but the results are otherwise similar to those for flame D. At $x/D = 15$ there is a significant number of local extinguished samples, with flame E having approximately 5 times that in flame D (not shown). At $x/D = 30$, the probability of local extinction is approximately 2-3 times lower than at $x/D = 15$ due to reignition as a result of the decay of the scalar dissipation rate (not shown).

The FMDF and the conditionally filtered diffusion involving $Y_{O_2}$ are shown with the $\xi$ axis plotted differently for clarity. Due to partial premixing mixing, the FMDF at $x/D = 7.5$ (not shown) is similar to the inverted FMDF of $\xi$, $T$ and $Y_{CO_2}$, with higher $Y_{O_2}$ values for both lean and rich mixtures but low values near $\xi_s$. The FMDF, although not in a plane, is largely limited to a two-dimensional manifold. At $x/D = 15$ (not shown), for small SGS variance the FMDF is again similar to the inverted FMDF containing $Y_{CO_2}$. For large SGS variance (not shown), the extent of the rich side is reduced due to consumption. There are some samples with higher $Y_{O_2}$ at lower temperatures due to local extinction. At $x/D = 30$ the rich side has further diminished (not shown).

The FMDF of $\xi$, $T$, and $Y_{CH_4}$ at $x/D = 7.5$ is concentrated near equilibrium values (Fig. 3). The $CH_4$ levels on the lean side are very low. At $x/D = 15$ the FMDF extends to higher $Y_{CH_4}$ values and lower $T$ values (Fig. 3b). The FMDF also appear to be limited to a plane.

The FMDF for $T$ and $Y_{CO}$ at $x/D = 7.5$ are not far from the equilibrium values for these burning flamelets. For small SGS variance, the FMDF is concentrated on the lean side of the peak $Y_{CO}$ (Fig. 3a). There is a sharp drop of $Y_{CO}$ due to the consumption reactions. For large SGS variance, the FMDF consists of three segments, one on the rich side of the peak $Y_{CO}$ and two on the lean side (Fig. 3b). They connect four vertices that are not in the same plane; therefore, unlike that of $\xi$, $T$ and $Y_{CO_2}$, the FMDF of $\xi$, $T$ and $Y_{CO}$ is not limited to a two-dimensional manifold and must be represented in a three-dimensional scalar space. Thus, the mixing problem

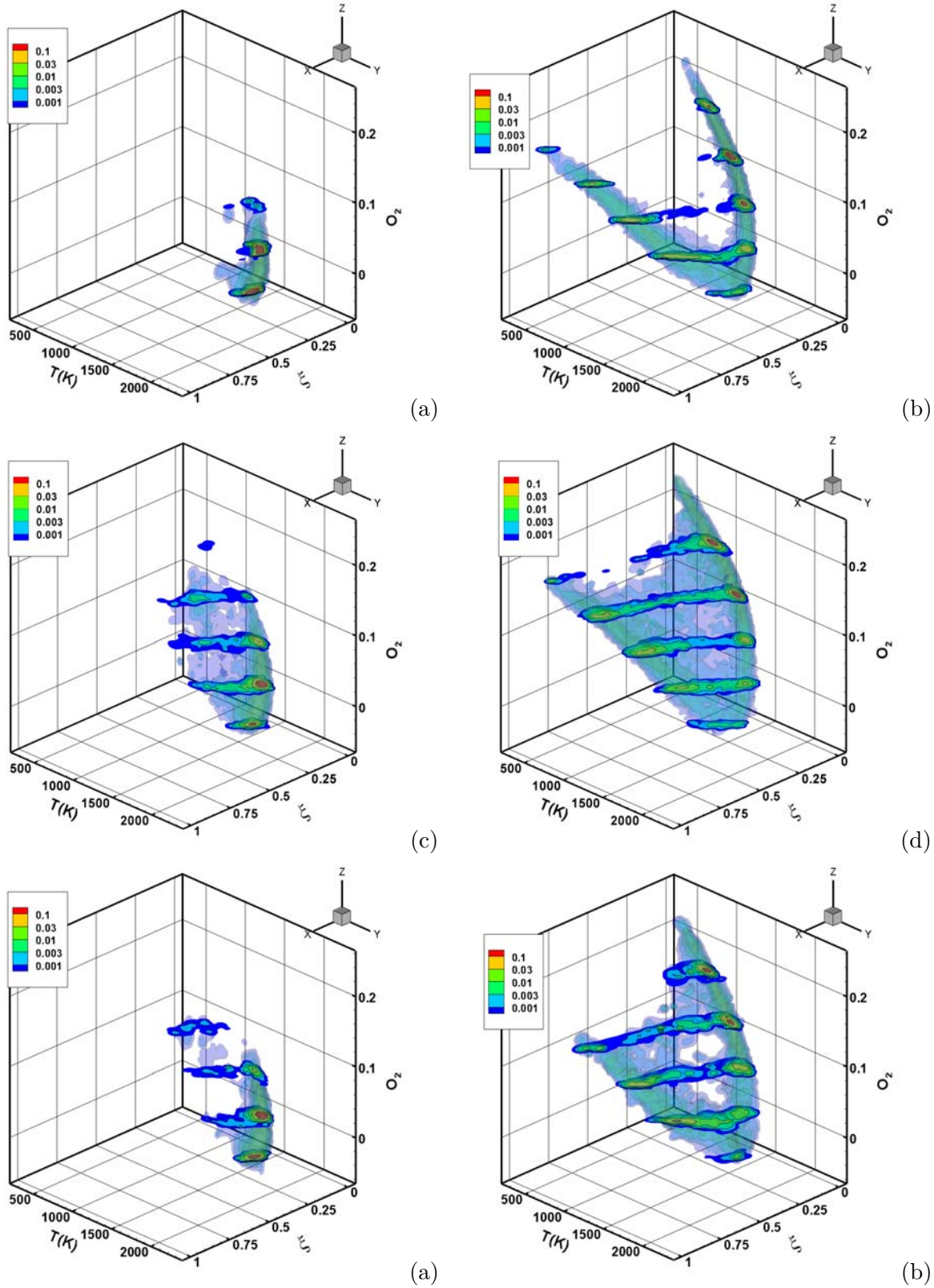


Figure 2: FMDF for $\xi$, $T$ and $Y_{O_2}$. Conditions same as in Fig. 1.

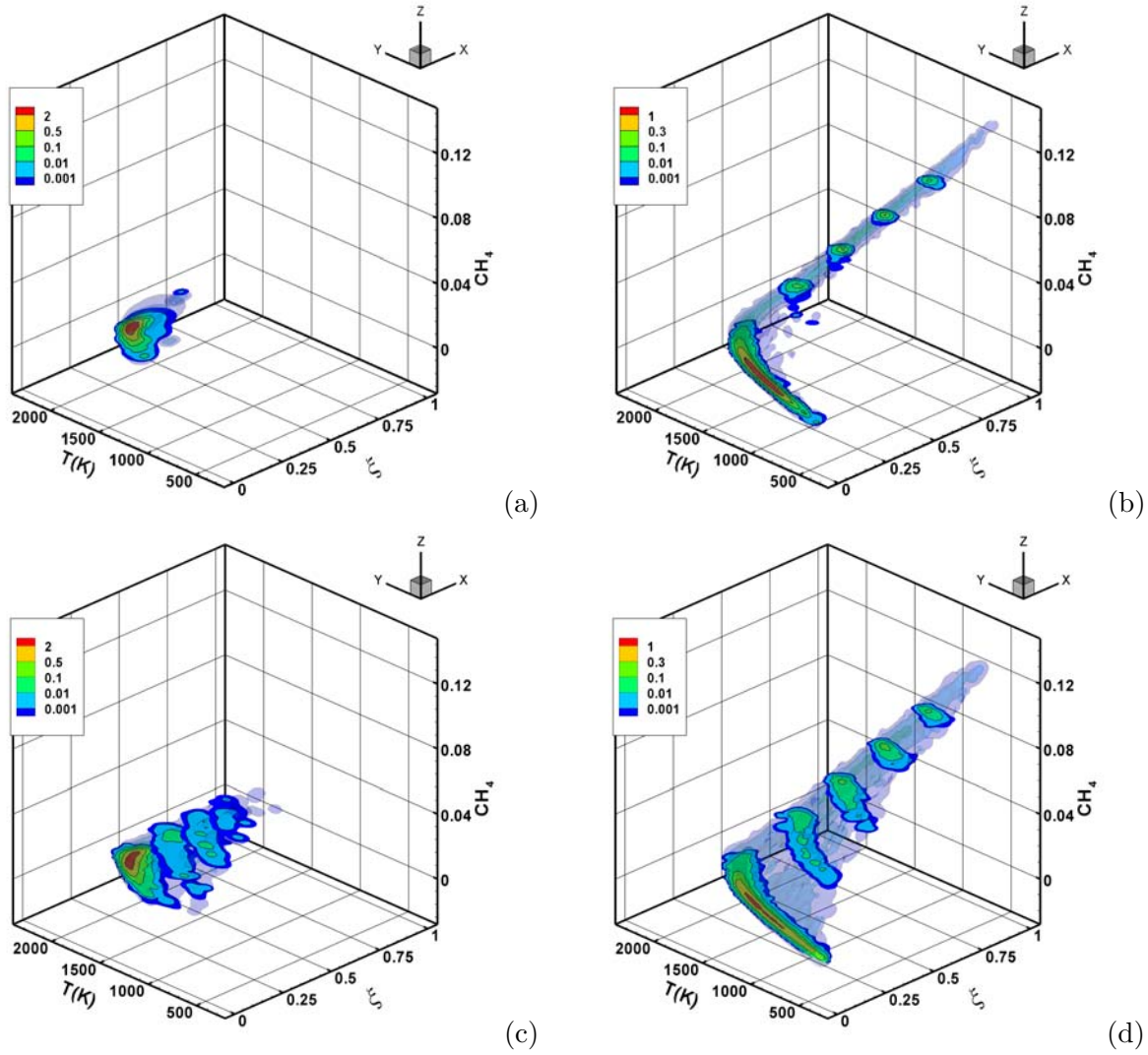


Figure 3: FMDF for $\xi$, $T$ and $Y_{CH_4}$. Conditions same as in Fig. 1.

is non-degenerated. On the far rich side the FMDF ridgeline is largely a straight line, due to the low reaction rates resulting in linear relationships among the scalars. The production rate of $Y_{CO}$ is highest near the peak, and is balanced by the negative diffusion. Just to the lean side of the peak $Y_{CO}$, where the consumption rate is highest, $Y_{CO}$ decreases rapidly to reach very low values at $\xi = 0.2$. Here the consumption rate is balanced by positive diffusion. Further to the lean side $Y_{CO}$ remains low and $T$ decreases linearly with $\xi$.

### B. The conditionally filtered scalar dissipation rates of species mass fractions

The conditionally filtered dissipation rate of $Y_{CO_2}$ for small SGS variance (not shown) generally is small near the stoichiometric mixture fraction, $\xi_s$, (0.351) and at high $CO_2$ (temperatures) levels. Away from $\xi_s$ as well as towards lower temperatures the dissipation increases, reaching the

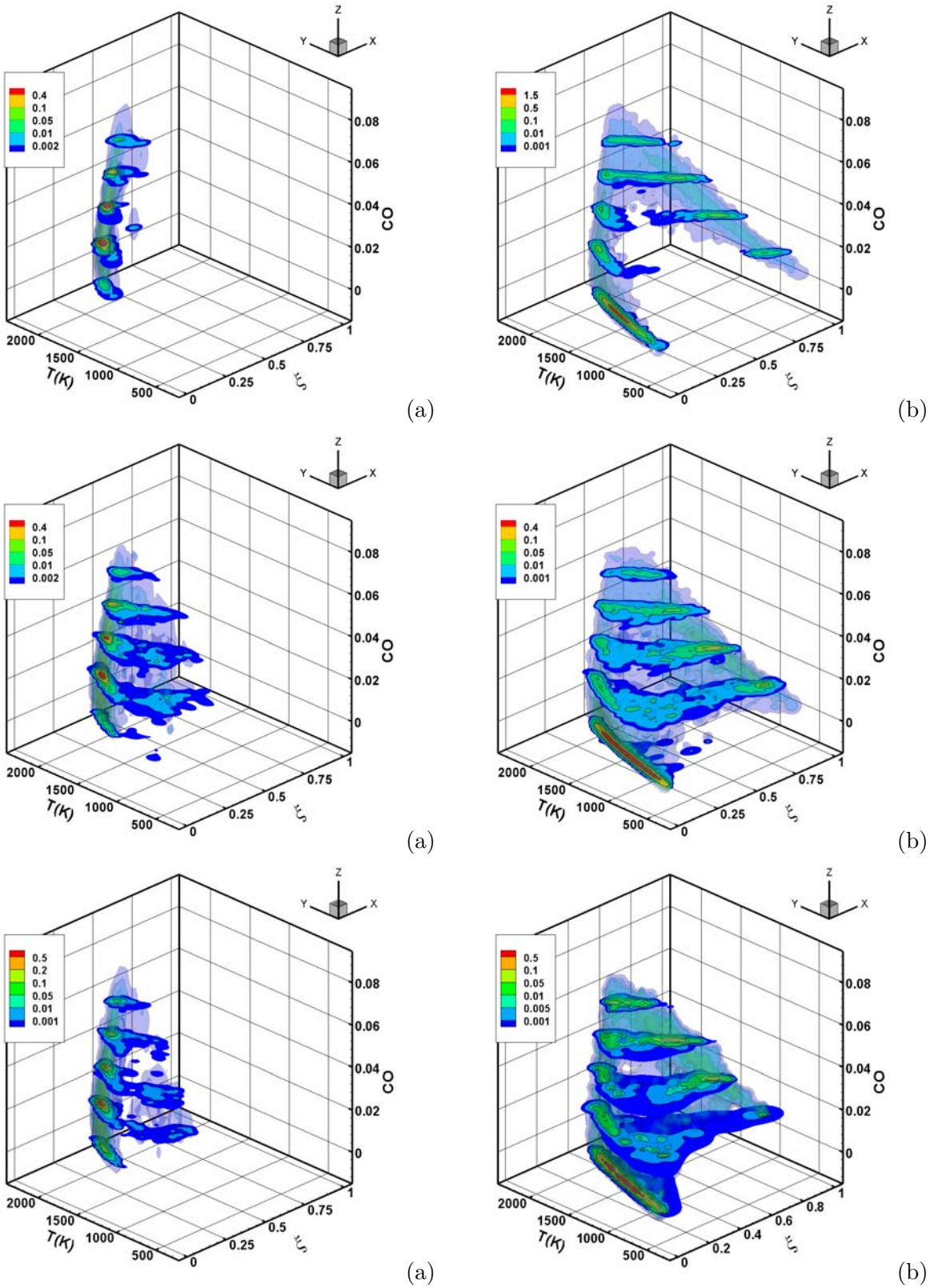


Figure 4: FMDF for $\xi$, $T$ and $Y_{CO}$. Conditions same as in Fig. 1.

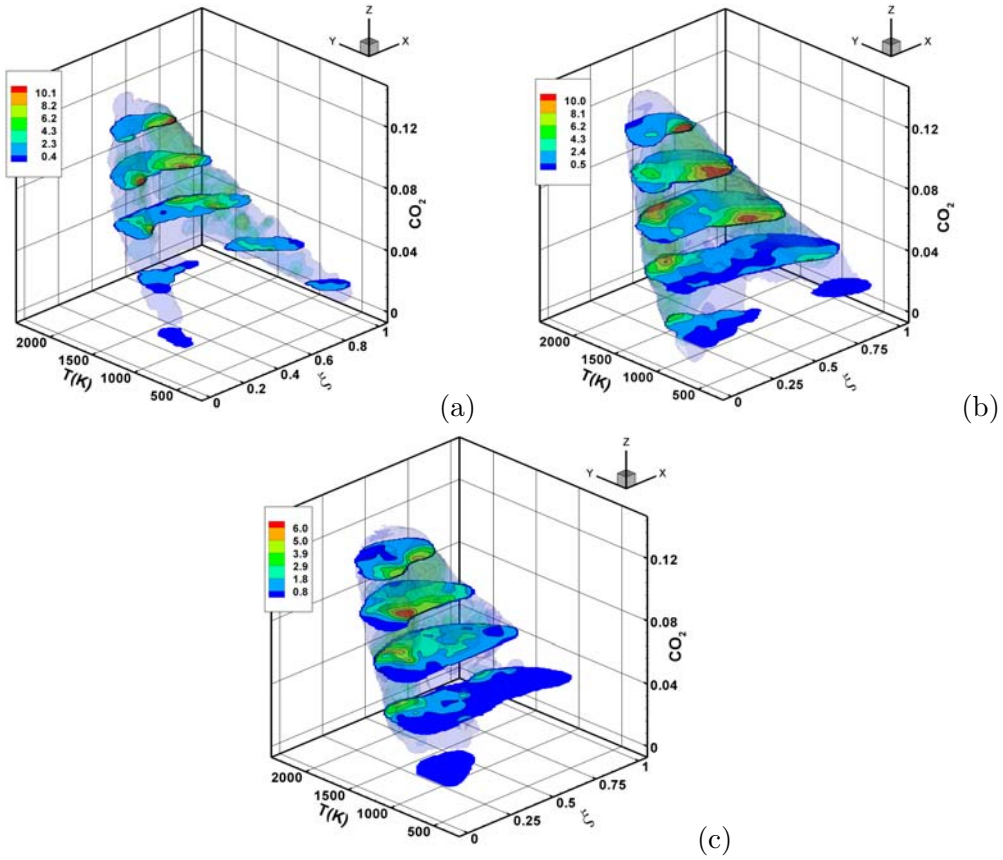


Figure 5: Conditionally filtered dissipation rate of $CO_2$ mass fraction in flame D. (a) x/D=7.5, $\langle \xi''^2 \rangle_L$=0.066; (b) x/D=15, $\langle \xi''^2 \rangle_L$=0.069; (c) x/D=15, $\langle \xi''^2 \rangle_L$=0.059; The Favre filtered mixture fraction is set to 0.35. The contours are obtained at $Y_{CO_2}$=0.0168, 0.0403, 0.0637, 0.0872, and 0.1106, respectively.

maximum near $Y_{CO_2} = 0.0637$ (at $x/d = 15$). The dissipation near $\xi_s$ at lower temperature (and $Y_{CO_2}$) is higher than near the peak $CO_2$, probably a result of the mixing between the burning and extinguished samples. These results generally are similar to the temperature dissipation rate [8] and are consistent with distributed reaction zones.

For large SGS variance, flame D at $x/d = 7.5$ primarily consists of fully burning flamelets. The dissipation (Fig. 1) is small near the peak $Y_{CO_2}$ and increases away from the peak, due to the $Y_{CO_2}$ and $\xi$ correlation. There are two maximums on either side of the peak, again consistent with flamelets. At $x/d = 15$, the burning samples have a dissipation rate distribution similar to that at $x/d = 7.5$. For the extinguished samples with lower $CO_2$ levels the dissipation rate decreases much faster near $\xi_s$ compared with small SGS variance, again reflecting the flamelet structure. At $x/d = 30$, the dissipation on the rich side is smaller than at $x/d = 15$ and is higher near $\xi_s$, likely due to reignition generating $CO_2$ and and its gradient. These results show that the dissipation for $CO_2$ is generally similar to that for the temperature in Ref. [8].

The $Y_{CO}$ dissipation rate for small SGS variance (not shown) is small near the peak CO location and to its rich side. Large dissipation values occur on the lean side of the peak. Here the scalar

dissipation depends weakly on the $\xi$ but $Y_{CO}$ decrease rapidly with $\xi$ due to its consumption (reaction sharpening of the gradient), resulting in large dissipation. The dissipation values for the extinguished samples at $x/d = 15$ are smaller but has a local maximum at intermediate CO levels, likely due to the mixing between burning and extinguished samples.

For large SGS variance, large dissipation values (Fig. 2) occur on the lean side of the $Y_{CO}$ peak. Here $Y_{CO}$ changes rapidly with $\xi$ and the scalar dissipation rate is large (due to the ramp-cliff structure), resulting in large $Y_{CO}$ dissipation rate (much larger than those for small SGS variance. At $x/d = 7.5$ there is little local extinction. The results are consistent with flamelets. At $x/d = 15$ the results for the burning samples are similar to those at $x/d = 7.5$. For the extinguished samples the CO mass fraction to the left side of the peak CO location is higher. The dissipation rate has local maximum values there. At $x/d = 30$ the results are similar to those at $x/d = 7.5$ due to reduced amount of local extinction.

The $Y_{CH_4}$ dissipation rate for small SGS variance (not shown) is small on the lean side and near $\xi_s$. It increases towards the rich side where $Y_{CH_4}$ is also higher. For large SGS variance, the dissipation at $x/d = 7.5$ is large on the lean side where the correlation between $Y_{CH_4}$ and $\xi$ is strong and the scalar dissipation is large. The results again are consistent with burning flamelets. At $x/d = 15$ large dissipation values occur at higher $Y_{CH_4}$ values and lower temperatures. This shift is due to the reduced consumption of $CH_4$ at lower temperatures.

The present work show that although four scalars are involved in the mixing of mixture fraction, temperature, and $CO_2$ (or $H_2O$), the mixing scenario is close to a three-stream mixing problem. The conditionally filtered dissipation rates for these variables are similar to that of temperature. On the other hand, mixing involving CO or $H_2$ is a four-stream mixing problem due to the four vertices in the scalar space. The conditionally filtered dissipation rates have different dependencies on the mixture fraction and temperature. These characteristics are interesting cases for testing mixing models.

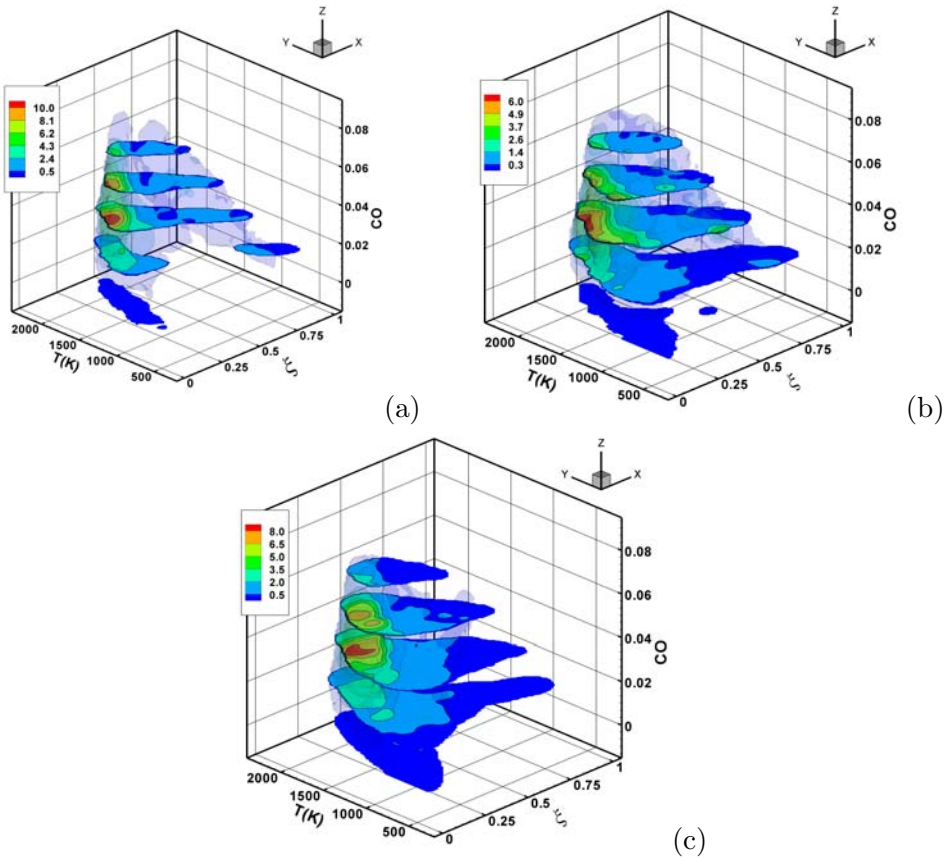


Figure 6: Conditionally filtered dissipation rate of CO mass fraction in flame D. (a) x/D=7.5; (b) x/D=15; (c) x/D=30. The Favre filtered mixture fraction and the SGS variance values are the same as in Fig. 5. The contours are obtained at $Y_{CO}$=0.0010, 0.0160, 0.0310, 0.0460, and 0.0610 respectively

### C. Conditionally filtered diffusion of mixture fraction, temperature, and species mass fraction

The diffusion velocity streamlines for $\xi$, $T$ and $Y_{CO_2}$ are shown in Figs. 1&2. For small SGS variance the streamlines at $x/D = 7.5$ generally converge first to a one-dimensional manifold, which is the ridgeline of the FMDF, and then continue towards a stagnation point. The diffusion velocity magnitude is larger during the approach to the manifold, indicating that the approach to the manifold is a faster process than the convergence to the stagnation point. This trend is similar to that for $\xi$ and $T$, and can be understood largely in the context of quasi-equilibrium distributed reaction zones, in which reactive scalar diffusion is closely coupled to the diffusion of the mixture fraction dissipation [9]. At $x/D = 15$ (Fig. 2c) the streamline for the burning samples are similar to those at $x/D = 7.5$. For the samples at lower $T$ and $Y_{CO_2}$, there is another stagnation point near $\xi = 0.4$, $T = 1600K$, and $Y_{CO_2} = 0.075$ (0.4, 1600K, 0.075). The mixing here is primarily between the burning and extinguished samples, and therefore is different from that for the samples

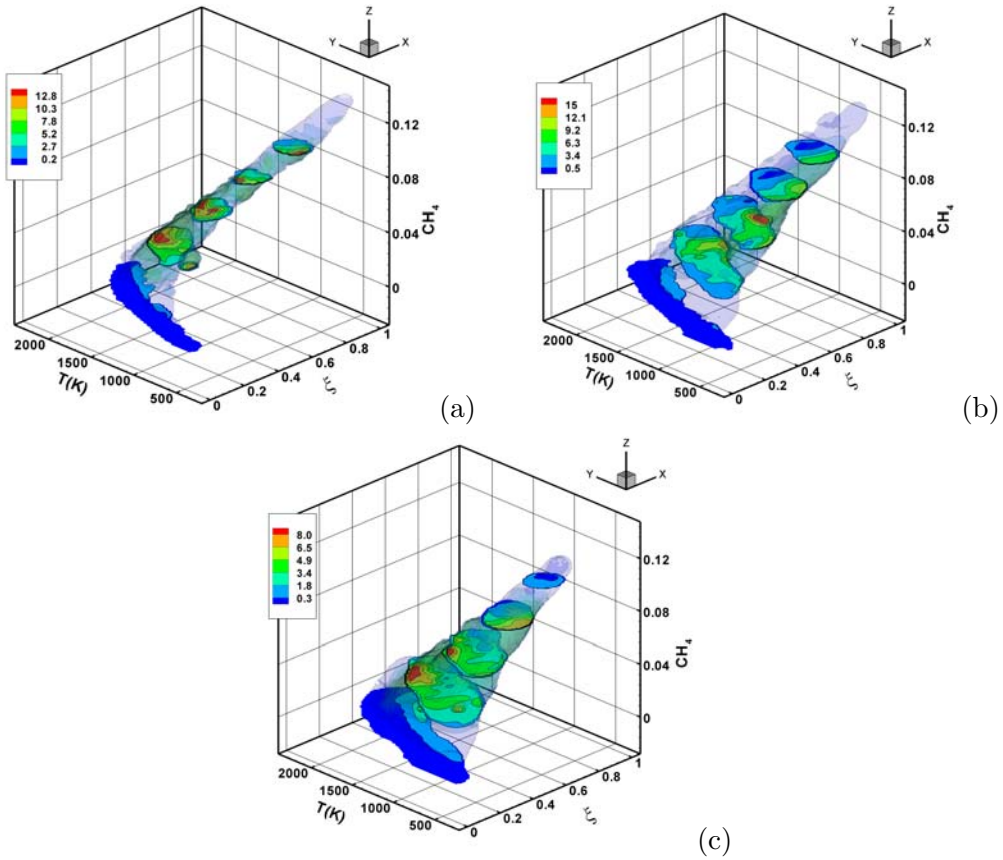


Figure 7: Conditionally filtered dissipation rate of $CH_4$ mass fraction in flame D. (a) x/D=7.5; (b) x/D=15; (c) x/D=15. The Favre filtered mixture fraction and the SGS variance values are the same as in Fig. 5. The contours are obtained at $Y_{CH_4}$=0.008, 0.031, 0.054, 0.077, and 0.080, respectively

near equilibrium. The results for $x/D = 30$ is similar to those at $x/D = 15$ (not shown).

For large SGS variance at $x/D = 7.5$ the streamlines for very rich ($\xi > 0.6$) and lean ($\xi < 0.2$) mixtures generally move in the direction of the ridgeline of the FMDF (Fig. 1d) towards the stoichiometric mixture fraction. For strained flamelets the mixture fraction profiles have an approximately error-function shape (ramp-cliff structure). Thus, the diffusion of $\xi$ is towards the center of the profiles (appears to be near $\xi = 0.45$). For very rich and lean mixtures $T$ and $Y_{CO_2}$ depend approximately linearly on $\xi$; therefore, their diffusion is proportional to the $\xi$ diffusion, resulting in straight diffusion streamlines along the ridgeline.

Near the peak $T$ and $Y_{CO_2}$ the $\xi$ diffusion is small because this region is close to the center of the error-function profiles where the curvatures of the profiles are small. The $T$ diffusion and $Y_{CO_2}$ diffusion are negative due to the negative curvatures of their profiles (as a function of $\xi$) and the approximately linear $\xi$ profiles. Consequently, the streamlines starting from the equilibrium curve near $\xi = 0.45$ move towards lower $T$ and $Y_{CO_2}$ values. As the streamlines move towards

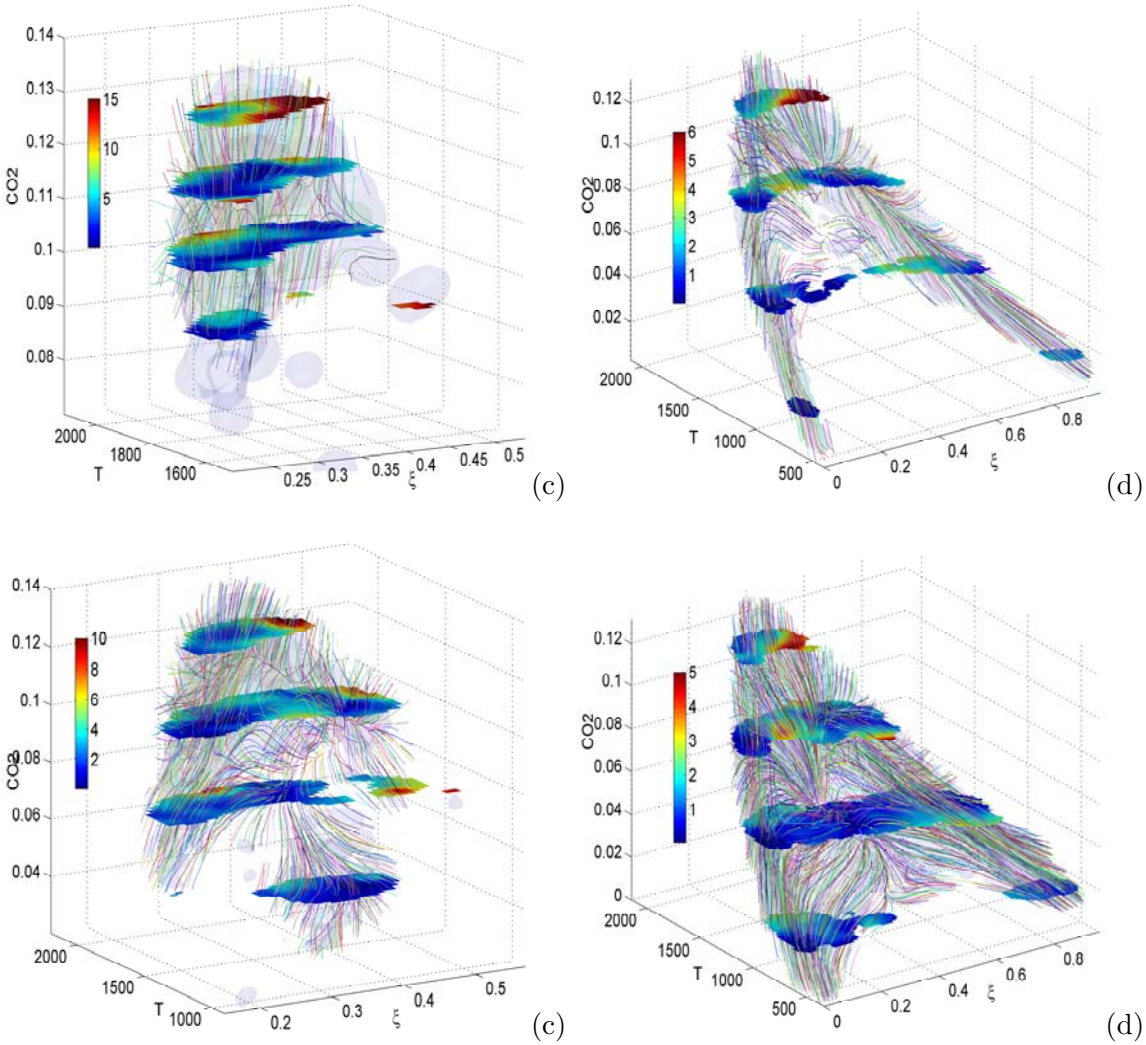


Figure 8: FMDF and diffusion velocity streamlines for $\xi$, $T$ and $Y_{CO_2}$ at $x/D = 7.5$ in flame D. (a & c) small SGS variance ($\langle\langle\xi''^2\rangle_L\rangle = 0.0013$, $\langle\langle\xi''^2\rangle_L\rangle = 0.0272$); (b & d) large SGS variance ($\langle\langle\xi''^2\rangle_L = 0.066$). The gray scales on the horizontal planes represent the magnitude of the diffusion v velocity vectors.

lower temperatures, the scalar dissipation rate increases, corresponding to more strongly strained flamelets and higher diffusion. The largest magnitude of the diffusion velocity vector occurs near $T = 1600 - 1800K$. Below this temperature range $T$ and $Y_{CO_2}$ profiles become broader (smaller curvatures) in the $\xi$ space, resulting in lower $T$ diffusion and $Y_{CO_2}$ diffusion. There appears to be a stagnation point at (0.4, 1300K, 0.058). Note that although this point appears to be the "center" of diffusion, it does not correspond to the conditional mean temperature and conditional mean $Y_{CO_2}$ for this mixture fraction value. Since the FMDF is transported by both diffusion and reactions, their combined action keeps the FMDF in the FMDF manifold. Individually they generally transport the FMDF out of the manifold unless one of them is small. Near the peak temperature both the reaction rates and diffusion are large, thus the diffusion streamlines move out of the FMDF manifold.

The streamlines starting from the very rich and lean regions move up along the ridgeline and turn near (0.27, 1600K, 0.082) and near (0.55, 1600K, 0.0760), respectively, towards the stagnation point. The $T$ and $Y_{CO_2}$ diffusion changes sign near these points, where the inflection points of $T$ and $Y_{CO_2}$ profiles are located. Below these points the diffusion is dominated by mixing whereas above it the diffusion is strongly influenced by both mixing and reaction. This streamline pattern is also consistent with the structure of flamelets.

At $x/D = 15$, the overall diffusion pattern for the burning samples (Fig. 2d) is similar to that at $x/D = 7.5$. For the extinguished samples the diffusion streamlines move primarily in the direction of mixture fraction towards $\xi \approx 0.4$, with only modest increases in $T$ and $Y_{CO_2}$. These trends indicate that for these samples the $\xi$ diffusion is initially much faster than $T$ diffusion. Previous results [9] have shown that this trend is due to extinguished flamelets. Near $\xi = 0.4$ streamlines move largely in the direction of $T$ and $Y_{CO_2}$ towards higher values. This $\xi$ value is close to the center of the ramp-cliff structure where the $\xi$ diffusion is small. For each flamelet, the $T$ and $Y_{CO_2}$ diffusion is negative at this mixture fraction. Thus, the observed positive $T$ and $Y_{CO_2}$ diffusion is likely due to the interaction between burning and extinguished flamelets resulting in diffusion along the iso-mixture fraction surface. At $x/D = 30$ the results (Fig. S3d) are similar to those at $x/D = 15$. The results for flame E are qualitatively similar to those for flame D at $x/D = 15$ and 30 except the earlier onset of local extinction (Fig. S15-S17). The results for $H_2O$ are similar to $CO_2$ and are not shown.

At $x/D = 7.5$ the diffusion streamline pattern (not shown) involving $Y_{O_2}$ is similar to the inverted streamlines involving $Y_{CO_2}$. Moving downstream to $x/D = 15$, for small SGS variance, the streamlines converge to the stagnation points (not shown). For large SGS variance, the streamlines (not shown) are also similar to the inverted streamlines for $Y_{CO_2}$, but those on the rich side start from lower $Y_{O_2}$ values than at $x/D = 7.5$. At $x/D = 30$, the streamlines start from even lower $Y_{O_2}$

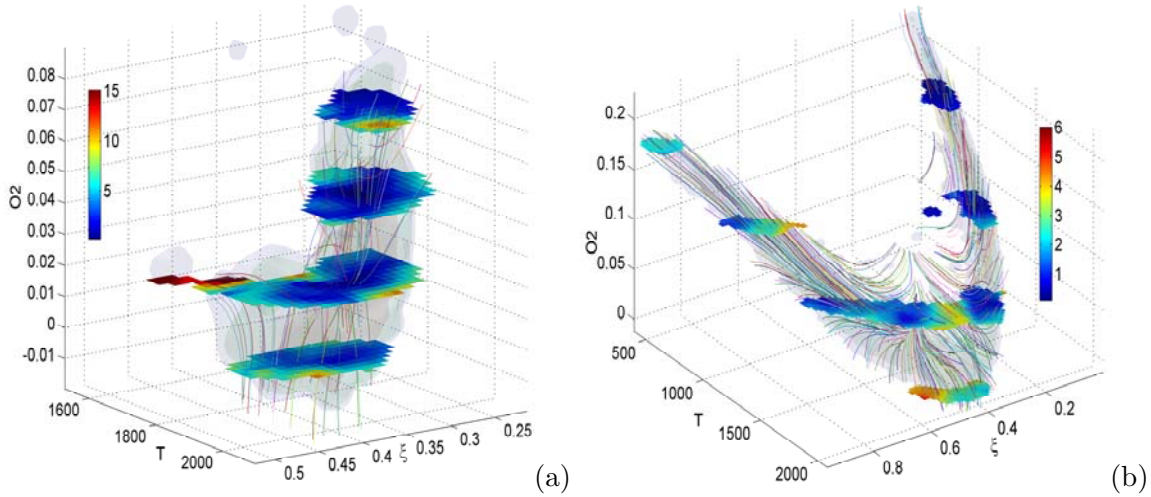


Figure 9: Diffusion velocity streamlines for $\xi$, $T$ and $Y_{O_2}$. Conditions same as in Fig. 8.

values (not shown).

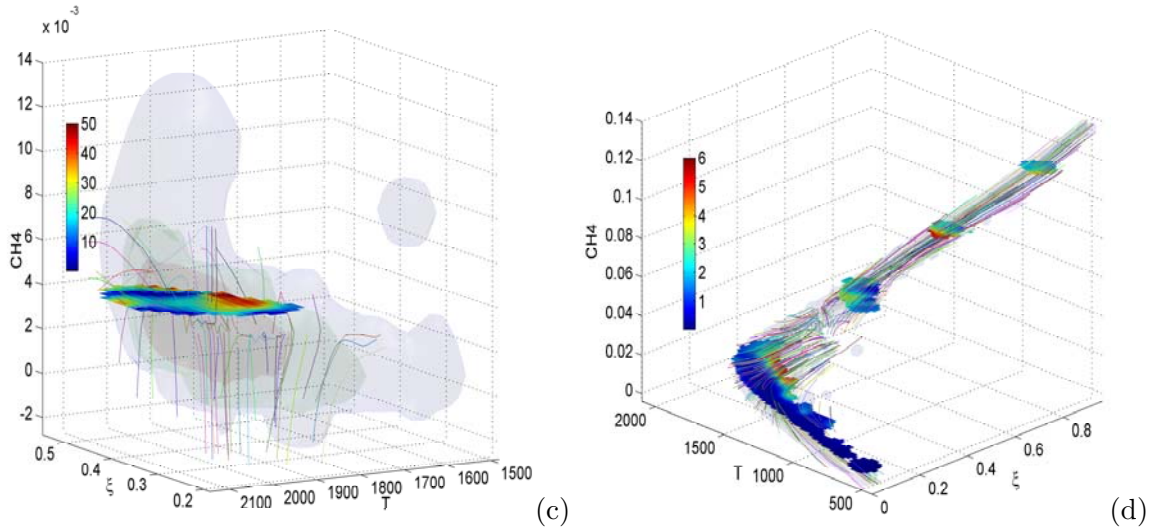


Figure 10: Diffusion velocity streamlines for $\xi$, $T$ and $Y_{CH_4}$. Conditions same as in Fig. 8.

The diffusion streamlines for $\xi$, $T$, and $Y_{CH_4}$ have a similar structure to those for $Y_{CO_2}$ (not shown). Near the peak temperature they move towards lower $T$ and higher $Y_{CH_4}$ values. The streamlines from the far rich and lean sides move along the FMDF ridgeline. For the extinguished samples the streamlines move towards $\xi = 0.4$ and then converge to a stagnation point.

$Y_{CO}$

For small SGS variance, the diffusion streamlines at $x/D = 7.5$ converge to a manifold and then to a stagnation point (Fig. 3c). At $x/D = 15$ (Fig. 4c) there is a second stagnation point at

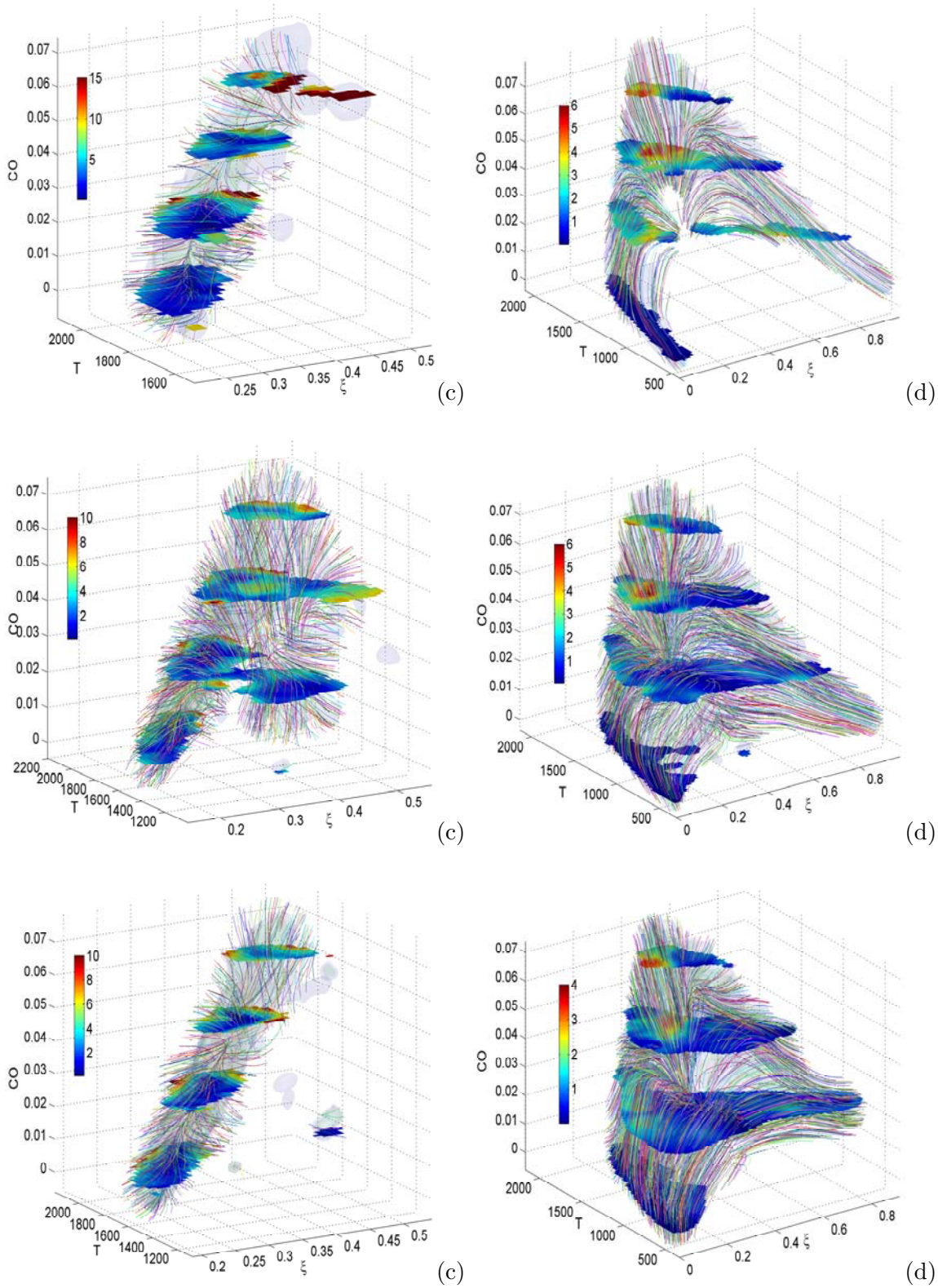


Figure 11: Diffusion velocity streamlines for $\xi$, $T$ and $Y_{CO}$. Conditions same as in Fig. 8.

lower $Y_{CO}$ values, towards which the streamlines converge. The results for $x/D = 30$ are similar. For large SGS variance at $x/D = 7.5$ (Fig. 3d) near the peak $Y_{CO}$, the diffusion streamlines move largely towards lower $T$ and $Y_{CO}$ values because of the negative curvature of the their profiles in flamelets. Here both the reaction rates and the negative diffusion are high and largely balance each other. Their combined action transports the FMDF within the FMDF manifold. Thus , the diffusion alone transports the FMDF out of the manifold, as shown in Fig. 3d. On the far lean side and the far rich side, the streamlines move along the ridgeline of the FMDF. Here the reaction rates are low, and the streamlines stay inside the FMDF manifold. On the lean side between 1000K to 1500K, the diffusion streamlines move towards higher $Y_{CO}$ but remain at approximately the same $T$. Due to the high CO consumption rate in these mixtures, the streamlines tend to move out of the FMDF manifold. The streamlines then turn towards lower $T$ and $Y_{CO}$, and converge to a stagnation point in the interior of the pyramid (not on the front or the back plane).

At $x/D = 15$ the streamline pattern for the burning samples are similar to that at $x/D = 7.5$ (Fig. 4d). For the extinguished samples, the streamlines from low $T$ and $Y_{CO}$ on the far lean side first move upward towards higher $Y_{CO}$. Here the reaction rates are low and the streamlines are located within the FMDF manifold (the left plane), which is generated by the diffusion. The streamlines then move towards $\xi_s$. On the rich side, the streamlines for the extinguished flamelets also move towards $\xi_s$, and together with those from the lean side forming the front plane. Since the reaction rates are low, the FMDF is transported in the direction of the streamlines. Near $\xi_s$ the streamlines move towards the stagnation point at higher $T$ and lower $Y_{CO}$. Again, for each flamelet the diffusion for both $T$ and $Y_{CO}$ is in the opposite direction of the streamlines. The diffusion here, therefore, is along the iso-mixture fraction surface ($\xi_s$), indicating diffusion among burning and extinguished flamelets. At $x/D = 30$, the overall streamline pattern is similar to that at $x/D = 15$ (not shown). The results for $H_2$ are generally similar to those of CO. One difference is that at $x/D = 15$ (not shown), the FMDF is broader than that of CO potentially due to higher noise as well as differential diffusion effects resulting from the higher diffusion coefficient of $H_2$.

The results show that the SGS mixing of $Y_{CO_2}$ and that of $Y_{CO}$ have significantly different characteristics. Being strongly correlated with the temperature, the SGS mixing of $Y_{CO_2}$ is similar to that of the temperature. The four-scalar ($\xi$, $T$, $Y_{CO_2}$, and co-flow $(1 - \xi)$) SGS mixing problem is similar to that of the three scalar ($T$, $Y_{CO_2}$, and co-flow) SGS mixing, and therefore, is a degenerated case. On the other hand, the SGS mixing of $\xi$, $T$, $Y_{CO}$, and co-flow is more complex because $Y_{CO}$ is depleted rapidly towards the lean side, resulting in a FMDF with four vertices that must be represented in a three-dimensional scalar space. Thus, the SGS mixing problem is non-degenerated. From a more general point of view, the different SGS mixing characteristics of $Y_{CO_2}$ and $Y_{CO}$ are a result of the different mixing configurations, i.e., the spatial relationships among

the scalars in physical space, which are closely tied to the chemistry: The peak location of $Y_{CO}$ approximately coincides with that of the temperature whereas the FMDF vertex near $\xi = 0.2$ is located between the co-flow and the peak temperature. In the Sandia flames the major species can be divided into several categories: $CO_2$ and $H_2O$, CO and $H_2$, $CH_4$, and $O_2$, each having a different spatial relationship with the mixture fraction, the temperature, and the co-flow. Except CO and $H_2$, the FMDFs for all the species have vertices near the peak temperature indicating relatively simple mixing configurations. In flames with more complex chemistry, additional mixing configurations may exist, resulting in different SGS mixing characteristics.

### D. Noise correction and resolution estimation for scalar dissipation rate measurements in turbulent partially premixed flames

In turbulent combustion research much effort has been devoted to measurements of the scalar dissipation rate. Because the scalar dissipation rate in a turbulent flame comes primarily from the smallest scalar length scales, its measurements require high spatial resolution. At the same time, the scalar fluctuations at these scales are generally much smaller than the energy-containing fluctuations, requiring low measurement noise to achieve an adequate signal-to-noise ratio for dissipation rate measurements. In practice, however, none of the two requirements is guaranteed. Often, the resolution of the measurement system is comparable to the smallest length scales, and the noise contribution to the dissipation rate is significant, potentially resulting in significant errors in the measured dissipation rate.

We recently developed a local analysis approach that uses conditional sampling[10, 11, 12] to evaluate the noise contributions. This method does not require redundant signals used in some previous studies and the assumption (or approximation) that the redundant signals are identical to the original signals. The method also does not rely on spectral analysis, allowing conditioning of the dissipation rate on the scalar value at the same location. The most important aspect of the method is the conditional sampling procedure, which is based on Kolmogorov's refined similarity hypotheses[13]. The procedure is used to select fully resolved (verified a posteriori) local scalar fields, effectively separating the noise effects from the resolution effects. The fully resolved local scalar fields then are used to determine the measurement noise. Because the conditional sampling procedure makes use of the properties of turbulent scalar fields, it essentially can guarantee selection of fully resolved local scalars, even when the whole scalar field is not fully resolved. The experimentally determined noise is applied to potentially under-resolved conditional local scalar fields for noise correction.

We used the conditional sampling technique that we developed to study SGS scalar mixing[10, 11, 14, 15, 12, 16]. The technique uses two conditioning variables: the filtered (locally averaged) scalar and the SGS scalar variance. The technique makes use of the properties of the turbu-

lent scalar fields. Our previous studies[10, 11, 14, 15, 12] have shown that for small SGS variance (smaller than mean SGS variance) the SGS scalar is well mixed. The statistics of such (conditional) fields are described well by the Kolmogorov-Obukhov-Corrsin theory. The locally averaged scalar dissipation rate and the scalar variance spectral transfer rate are lower than the mean scalar dissipation rate. In the spirit of the Kolmogorov's refined similarity hypotheses, the local conditional Peclet number is expected to be lower than that based on the unconditioned statistics; therefore, the scalar dissipation length scales for these fields are expected to be larger than the mean scalar dissipation length scale. By choosing sufficiently small SGS variance values, one can select local scalar fields with large dissipation length scales so that they are resolved well by the measurement apparatus. This property of the local turbulent scalar fields is demonstrated by the experimental results (Fig. 11).

For large SGS variance, the locally averaged conditional scalar dissipation rate and the spectral transfer are larger than their mean values. In addition, the SGS scalar is highly segregated and contains the so-called ramp-cliff structure[17, 11, 14, 12]. The scalar dissipation rate is very large inside the cliffs. At the same time, the cliffs in the SGS scalar are likely to have smaller length scales. Using conditional sampling with large (much larger than the average SGS variance) SGS variance values, one can select local scalar fields that potentially are under-resolved to evaluate their dissipation length scales. These fields can be analyzed to determine the dissipation length scales and to correct for any under-resolution. Because this method makes use of the physics of the turbulent scalar fields, it does not require redundant measurements.

To obtain the scalar dissipation rate numerical (usually finite difference) schemes are needed to calculate the derivatives because experimental data are generally discrete samples. Different schemes involve different numbers of samples and different weights to the samples. Consequently, the calculated scalar dissipation rate and the noise contribution are scheme dependent.

In this method we make use of the different spectral response (or resolution) of finite difference schemes (or numerical stencils) of different order in determining the measurement noise and evaluating the measurement resolution; therefore, unlike some of the previous methods, this method does not rely on varying the measurement resolution (or the sample spacing) to evaluate dissipation length scale, and only one resolution is needed.

In this study we used the assumption that the noise at different measurement locations (be it different samples from a single probe or pixels of an imaging device) is uncorrelated and is additive to the scalar values.

$$\xi = \xi^* + n \tag{5}$$

where $\xi^*$, $\xi$ and $n$ are the true scalar value, the measured value, and the noise, respectively. To

correct for the noise contribution to the measured dissipation rate the noise variance needs to be determined.

For the Sandia flame data used in the present work, the measurement noise is dominated by shot noise. The mixture fraction was calculated using Bilger's formula with C and H elemental mass fractions. Oxygen was excluded due to its high experimental uncertainty. All the major species mass fractions except CO were measured using Raman scattering. Due to the lower Raman signal/noise ratio these measured mass fractions have higher noise levels than the CO mass fraction measured by the two-photon laser-induced fluorescence (LIF) technique; therefore, the noise variance for the mixture fraction is dominated by the noise from the species measured by Raman scattering. Because the C and H atoms both originated from the fuel stream we expect the noise variance to increase with the mixture fraction. With this consideration we modeled the noise variance as proportional to the mixture fraction. Because the noise variance for the well resolved local scalar is determined near the stoichiometric mixture fraction, $\xi_s$, the model essentially evaluates the variations from that value. We also have tested a model that is locally constant with respective to the mixture fraction. The results show that the scalar dissipation length scales inferred using our approach are not sensitive to the details of the noise model, probably because the finite difference schemes involve samples with both lower and higher noise variances than that at the location where the derivative is calculated, partially canceling the effects of the variations in the noise variance; therefore, this simple model appears to be sufficiently accurate for the noise corrections.

To account for the dependence of the noise variance on the temperature we considered only the dependencies of the Raman scattering cross-sections on the mixture density but not on the the mixture compositions. Because the species number densities are proportional to the mixture density, so are the total scattering cross-section (signal) and the noise variance. Consequently, the model noise variance for the normalized signal ($\xi$) is inversely proportional to the density and is proportional to the temperature for low-speed flows. The variance of noise then is modeled as proportional to both the mixture fraction and the temperature,

$$\langle n^2 | \hat{\xi}, \hat{T} \rangle = \sigma_n^2(\hat{\xi}, \hat{T}) = B \cdot \xi^* \cdot T^* \tag{6}$$

By including this noise model in the finite difference scheme the measured derivative is

$$\begin{aligned} h \cdot \widetilde{\frac{d\xi}{dx}} &= a_1(\xi_1 - \xi_{-1}) + a_2(\xi_2 - \xi_{-2}) + a_3(\xi_3 - \xi_{-3}) + a_4(\xi_4 - \xi_{-4}) + \dots \\ &= a_1(\xi_1^* - \xi_{-1}^*) + a_2(\xi_2^* - \xi_{-2}^*) + a_3(\xi_3^* - \xi_{-3}^*) + a_4(\xi_4^* - \xi_{-4}^*) + \dots \\ &\quad + a_1 n_1 - a_{-1} n_{-1} + a_2 n_2 - a_{-2} n_{-2} + a_3 n_3 - a_{-3} n_{-3} + a_4 n_4 - a_{-4} n_{-4} + \dots \\ &= h \cdot \widetilde{\frac{d\xi^*}{dx}} + a_1 n_1 - a_{-1} n_{-1} + a_2 n_2 - a_{-2} n_{-2} + a_3 n_3 - a_{-3} n_{-3} + a_4 n_4 - a_{-4} n_{-4} + \dots \end{aligned} \tag{7}$$

where $\widetilde{\frac{d\xi^*}{dx}}$ is the estimated derivative without noise. Such an estimated derivative is dependent on the scheme used due to the different spectral responses. The measured mean dissipation rate is

$$\begin{aligned}
\langle\tilde{\chi}\rangle &= \left\langle 2D\Big(\widetilde{\frac{d\xi}{dx}}\Big)^2\right\rangle \\
&= \left\langle 2D\Big(\widetilde{\frac{d\xi^*}{dx}}\Big)^2\right\rangle + \left\langle \frac{2D}{h^2}\sum_{i=-N}^{N} a_i^2 n_i^2\right\rangle \\
&= \left\langle 2D\Big(\widetilde{\frac{d\xi^*}{dx}}\Big)^2\right\rangle + \frac{2\langle D\rangle}{h^2}\Big\langle \sum_{i=-N}^{N} a_i^2 n_i^2\Big\rangle \\
&= \left\langle 2D\Big(\widetilde{\frac{d\xi^*}{dx}}\Big)^2\right\rangle + \frac{2\langle D\rangle}{h^2} B \sum_{i=-N}^{N} a_i^2 \langle \xi_i^* T_i^*\rangle \\
&\approx \left\langle 2D\Big(\widetilde{\frac{d\xi^*}{dx}}\Big)^2\right\rangle + \frac{2\langle D\rangle}{h^2} B \sum_{i=-N}^{N} a_i^2 \langle \xi_i T_i\rangle \qquad (8)
\end{aligned}$$

where $C_N = \sum_{i=-N}^{N} a_i^2\langle\xi_i T_i\rangle$, $D$, and $2D\Big(\widetilde{\frac{d\xi^*}{dx}}\Big)^2$ are a scheme dependent factor, the molecular diffusivity, and the estimated dissipation rate without noise, respectively.

When all the schemes can resolve the turbulence scalar field, the measured mean dissipation rate $\left\langle 2D\Big(\widetilde{\frac{d\phi^*}{dx}}\Big)^2\right\rangle$ does not depend on the scheme; therefore, the measured mean dissipation rate vs. $C_N$ is a straight line with a slope of $\frac{2D}{h^2}\langle n^2\rangle$ and an intercept equal to the noise-corrected dissipation rate. This linear relationship can be used to determine the noise variance $\langle n^2\rangle$.

When the resolution is reduced, the measured dissipation rate obtained using the second-order scheme will be the first to fall below the straight line because it is least capable of resolving the dissipation rate. The deviation from the linear relationship will be followed by the fourth- and higher-order schemes as the resolution is further reduced; however, as long as the eighth- and tenth-order schemes follow this straight line, the dissipation still is resolved fully. The $\langle\chi\rangle - C_N$ plot also can be used, therefore, to determine whether or not the scalar dissipation is resolved fully. We employed the conditional sampling method to select fully resolved local scalar fields and to determine the noise variance according to Eq. 9. The noise variance then was used to correct the dissipation rate from potentially under-resolved local scalar fields. The noise-corrected dissipation rates from the different schemes then were analyzed to evaluate the scalar dissipation length scales and to correct for the resolution effects.

In this study we used the Favre-filtered (locally averaged) scalar and the Favre SGS scalar variance as conditioning variables. The conditionally filtered dissipation rates were calculated using five central difference schemes. As the scheme order increased, the conditionally filtered dissipation rates increased. Figure 12 shows that in Flame D at $x/D = 15$ for $\langle\xi\rangle_L = 0.35$ and $\langle\xi''^2\rangle_L = 5.2\times10^{-4}$ (small SGS variance), the $\langle\langle\chi|\xi\rangle|\langle\xi\rangle_L, \langle\xi''^2\rangle_L\rangle - C_N$ plot forms a straight line,

indicating that for small SGS variance, the scalar fields were well resolved by all the schemes. The noise-corrected conditionally filtered dissipation (the intercept) is of the same order as the noise contributions, indicating that the method is capable of accurately determining the noise variance even when the noise contribution is larger than the true dissipation rate.

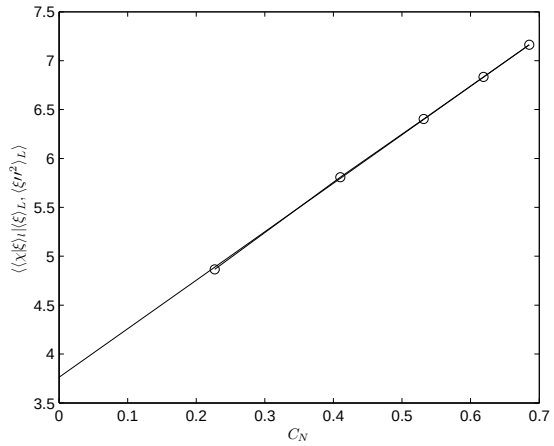


Figure 12: Dissipation rates vs $C_N$ in D15, $\langle\xi''^2\rangle_L = 5.2 \times 10^{-4}$

From Fig. 11 the noise variance and $B$ in Eq. 9 can be determined for flame D at $x/D = 15$. For small SGS variance values the fluctuations in both the mixture fraction and the temperature were small; therefore, the noise evaluation for the well-resolved scalar fields does not depend on the specific noise model used, as long as the noise variance is a function of the mixture fraction and the temperature.

For large SGS variance, $\langle\xi''^2\rangle_L = 6.7 \times 10^{-2}$ (Fig. 13), the conditionally filtered dissipation rates using the sixth- and lower-order schemes are below the straight line formed by the eighth-and tenth-order schemes, indicating that the sixth- and lower-order schemes are not capable of resolving all the scalar length scales. The dissipation rate using the second-order scheme ($\sim 139s^{-1}$) is less than the intercept of straight line ($\sim 148.7s^{-1}$), indicating that even without correcting for noise, the second-order scheme is underestimating the dissipation rate; however, there is no evidence to show that whether or not eighth and tenth order schemes are capable of fully resolving the scalar scales. The true dissipation rate, therefore, is equal or higher than the intercept of the straight line.

After correcting for the noise, the measured dissipation rate is affected only by the resolution, which is expected to be the worst when the SGS scalar variance is large due to the sharp cliffs in the SGS scalar. Because the scalar dissipation length scales were not known *a priori*, we needed to use experimental data to infer them. Comparing the measured scalar spectrum to a model spectrum

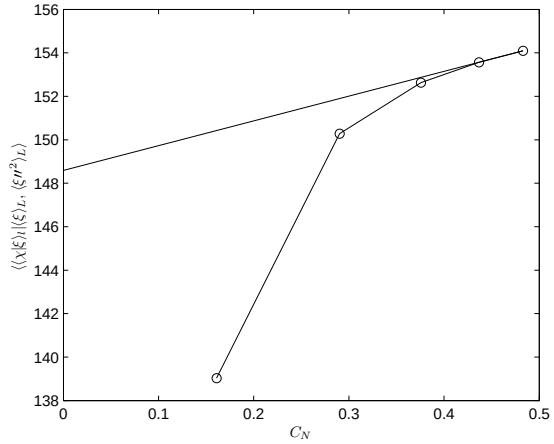


Figure 13: Dissipation rates vs $C_N$ in D15, $\langle\xi''^2\rangle_L = 6.7 \times 10^{-2}$

can provide an estimate of the average length scale, but not that of the cliffs, which dominate the scalar dissipation rate for large SGS variance. To estimate the length scales of the cliffs we used the error function as a model for the ramp-cliff structure in the SGS scalar field and calculated the dissipation rate using different schemes with a range of sample intervals (spatial resolutions).

We used the ratios of the dissipation rates calculated using different schemes to infer the scalar dissipation scales. By equating the ratios from the measured dissipation rates and from the model, a scalar dissipation scale was inferred. The ratios of dissipation rates are shown in Figure 14. The ratios for the highest dissipation rate (at $\xi = 0.5$) are shown and are compared with the error-function model because these ratios correspond to the smallest scalar length scale. The horizontal axis is the ratio of sample distance to the scalar profile width, $h/w$. The ratio of the second-order to the tenth-order estimations is approximately 0.84, giving a $h/w$ of 0.52. The scales inferred from all the other schemes also agree very well, indicating the overall success of the noise correction and resolution/length scale evaluation. At this sample interval, figure 15 shows that the second-order scheme under-estimated the dissipation rate by 16%, the sixth-order scheme by 2%, and the eighth- and tenth-order by less than 1%; therefore, a sample interval of approximately 0.5 $w$ is sufficient to resolve the dissipation rate.

The resolution correction considered here is for large SGS variance, corresponding to the largest dissipation rate. The method in the present study can be applied to the mean scalar dissipation rate by summing the corrected dissipation rate for each SGS variance values weighed by the probability for each SGS variance value. Because the resolution improved with decreasing SGS variance, the percentage of the resolved mean dissipation is expected to be higher; therefore, the amount of correction for the mean dissipation rate will be smaller.

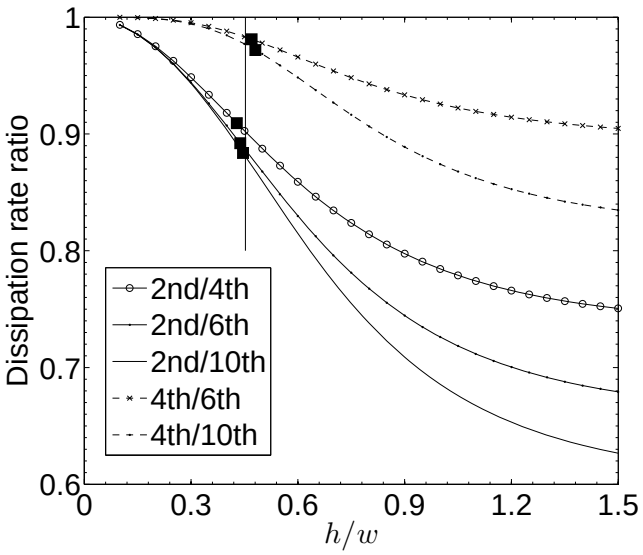


Figure 14: Estimation of the length scale by comparing the ratio of dissipation rate obtained from data (solid squares) to that from the model (curves). The ratios obtained using different schemes are shown.

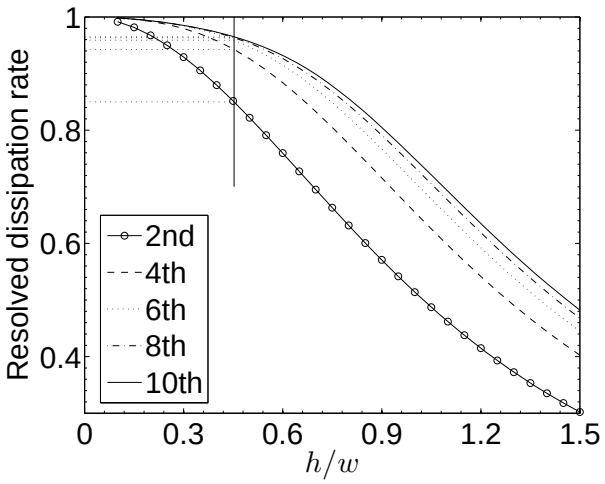


Figure 15: Estimation of the resolved dissipation rate obtained using the estimated length scale and the error-function model.

In the transport equation of the filtered joint density function of mixture fraction and temperature, one of the mixing terms is the scalar dissipation rate filtered conditionally on both mixture fraction and temperature. In this part we examine the dissipation length scale associated with this quantity and the extent to which they are resolved. We focus on the cases with large SFS variance when the smallest length scale and potential under-resolution occur.

When the SFS variance is large, the local SFS scalar fields can contain burning and extinguished flamelets. When the scalar dissipation rate increases, the temperature decreases; therefore, the scalar dissipation length scale is likely to decrease with temperature. The decrease can occur for two reasons: an increased strain rate that results in a higher dissipation rate, and a reduced scalar diffusivity at a lower temperature. As a result, when both the mixture fraction and temperature are used as conditioning variables, estimations of the resolution and length scale need to be performed for a range of temperatures. Here we evaluate the resolution for each error-function profile at the mixture value where the dissipation rate is least resolved. The length scale obtained, therefore, represents the smallest length scale for the dissipation rate.

We compute the ratio of the measured scalar dissipation rate obtained using the second-order scheme to that using the tenth-order scheme at each temperature for the entire range of mixture fraction (Fig. 16). The lowest point at each temperature represents the location (in the scalar space) of the least resolved portion of the scalar profile. This ratio is compared with the error-function model to obtain an $h/w$ value and to determine the fraction of the dissipation resolved. The results for Sandia flames D and E at the three downstream locations are shown in Fig 17. In general, $h/w$ decreases ($w$ increases) when the temperature increases, consistent with the properties of laminar flamelets. In some cases we limit the temperature to approximately 1800K, because very close to the equilibrium temperatures, the scalar field is well-resolved by both schemes. Thus the ratio is close to unity and is not sensitive to the $h/w$ value (Fig. 15). As a result, at these temperatures the statistical uncertainties in calculating the ratio can have a large impact on the inferred $h/w$ values (e.g., the ratio can exceed unity slightly, for which $h/w$ is not defined). In these cases, however, the scalar is well-resolved and the $h/w$ value is not needed to estimate the dissipation rate.

For flame D at $x/d = 7.5$ the $h/w$ value is approximately 0.30 at 1850K (Fig. 17), i.e., the width of the error-function profile is three times the sample spacing. The dissipation rate is more than 98% resolved by the tenth-order scheme (Fig. 18). The $h/w$ value increases to approximately 0.68 at 1300K, corresponding to approximately 91% resolution of the dissipation rate, and indicating that the measurement resolution is adequate, even for the highest dissipation rate at this location. Moving to $x/d = 15$, $h/w$ is also approximately 0.3 at 1800K, again indicating sufficient resolution. The temperature at this location, however, can drop much lower due to the local extinction events. At 700K, $h/w$ increases to nearly 1.0, corresponding to a much narrower

error-function profile due to both high strain rate and reduced diffusivity at low temperatures. Only 72% of the largest dissipation rate is resolved. At this location, the measurement resolution is capable of adequately resolving the dissipation rate down to 1300K. Further downstream at $x/d = 30$, where the dissipation rate has reduced, the maximum $h/w$, which occurs at 1000K, is less than 0.75, smaller than those at the upstream locations. Approximately 90% of the dissipation at this temperature is resolved.

The $h/w$ values for flame E are generally higher than those for flame D at the same downstream locations, reflecting the higher Reynolds number for the former. At $x/d = 7.5$ there is already a significant amount of local extinction. The $h/w$ value reaches 1.4 at 770K, the highest of all cases. Only 52% of the dissipation at this temperature is resolved, the least resolved case. Nonetheless, at 1800K, 98% of the dissipation is resolved because the flamelets are expected to be only mildly strained. At $x/d = 15$ and 30, the results are qualitatively similar to those for flame D, with the resolved dissipation rate a few percentages lower.

Overall the smallest length scale in flame E is smaller than that in flame D, consistent with the expected Reynolds number dependence. The results show that to fully resolve the smallest length scale associated with the conditionally filtered dissipation rate in these flames, the pixel size needs to be reduced by approximately one half.

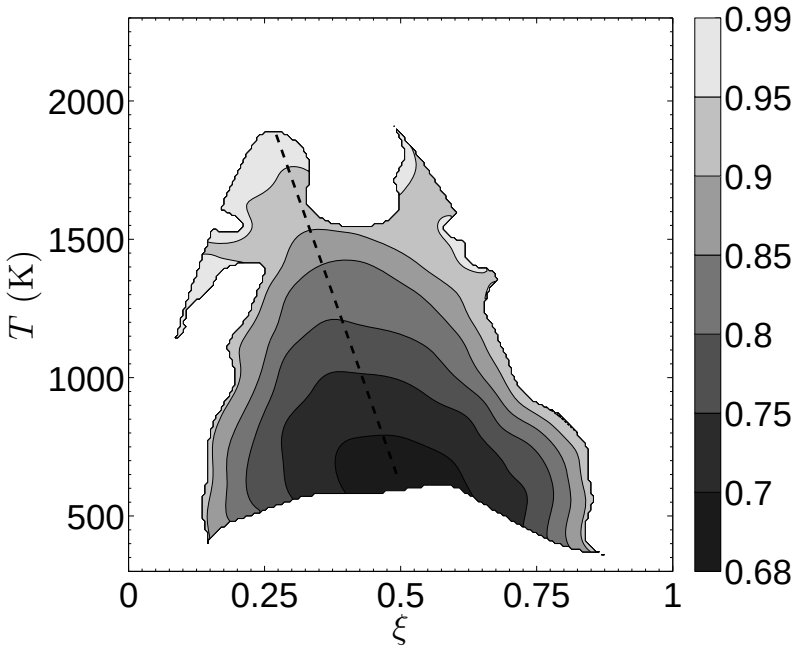


Figure 16: Ratio of the measured dissipation rate using the second-order scheme to that using the tenth-order scheme in flame D at $x/d = 15$. The lowest value at each temperature (near the dashed line) represents the least resolved part of the mixture fraction profile.

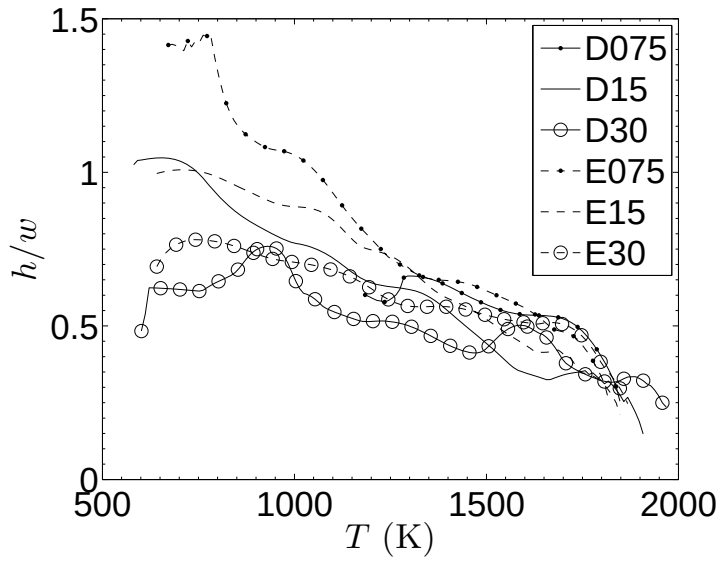


Figure 17: Length scale of the scalar (ramp-cliff) structure as a function of temperature. The SFS variance values are given in Fig. 8.

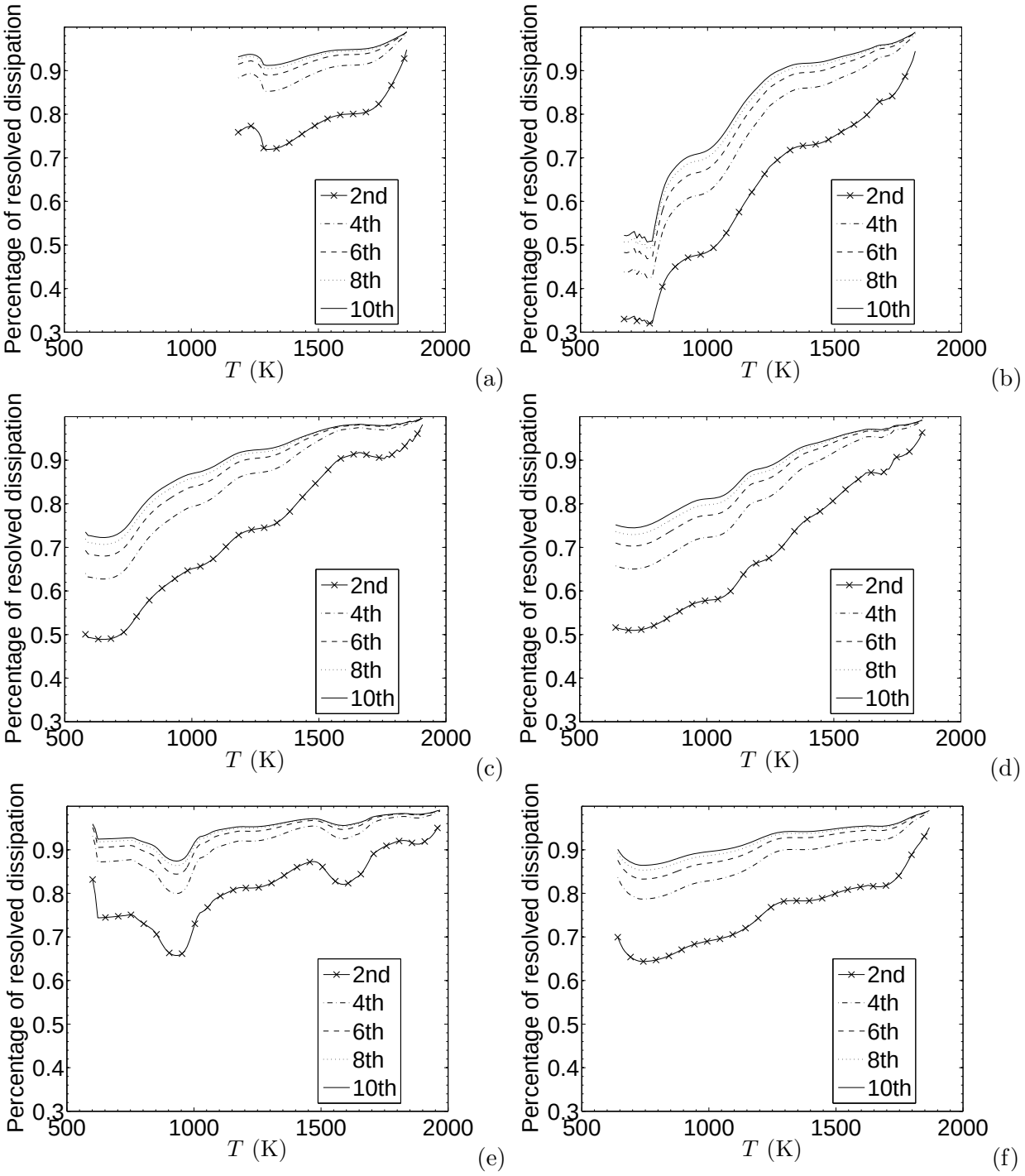


Figure 18: Estimation of the resolved dissipation rate as a function of temperature. (a), (c), and (e) flame D at $x/d$=7.5, 15, and 30, respectively; (b), (d), and (f): flame E at the same locations.

# IV Conclusions and suggestions for LES

The results obtained in this research significantly advanced the understanding of the SGS mixing of the mixture fraction (a conserved scalar) and temperature (a reactive scalar), which is important for modeling SGS mixing in LES of turbulent combustion. The issues investigated include the scalar FMDF and its transport equation, the scalar-temperature FMDF, and the FMDF transport equation. We also developed and tested a conditional sampling-based method for noise and resolution corrections for scalar dissipation rate measurements. The specific conclusions and suggestions for LES are:

- The mixture fraction FMDF is unimodal for small SGS scalar variance regardless of the filter scale. The conditionally filtered scalar dissipation rate depends weakly on the SGS scalar, indicating that the SGS scalar is well mixed; therefore, such a SGS mixture fraction is likely to result in distributed reaction zones.

- For large SGS variance the FMDF becomes bimodal, and the conditionally filtered scalar dissipation is bell-shaped, indicating the existence of a ramp-cliff structure, which is similar to the mixture fraction profile in the counter-flow model for laminar flamelets. The SGS mixing fields under such conditions, therefore, support flamelets.

- At a given location the SGS flame fluctuated between distributed reaction zones and laminar flamelets in the flames studied. Laminar flamelets contributed to nearly 50% of the heat release, further highlighting their importance in flames and the need for mixing models to capture the bimodal FMDF.

- The mixture-fraction-temperature FMDF also has qualitatively different shapes for small and large SGS variance. For small SGS variance the FMDF is unimodal, but for large SGS variance it is bimodal, with the two peaks outside of the reaction zone.

- The conditionally filtered mixture fraction dissipation for small SGS variances is generally consistent with quasi-equilibrium distributed reaction zones with a relatively weak dependence on the mixture fraction. For the extinguished samples the dissipation is not very large and is not sensitive to the temperature, suggesting that these samples may be extinguished at some upstream locations.

- For large SGS variance, the dissipation is large near $\xi = 0.4$, where the maximum gradient in a cliff is located. The dissipation is higher for lower temperatures, consistent with strained laminar flamelets. For the extinguished samples, the measured dissipation rate com-

ponent exceeds the extinction dissipation rate. The results indicate that these samples were extinguished flamelets.

- The conditionally filtered temperature dissipation for small SGS variances has a minimum (close to zero) near the peak temperature. For the extinguished samples with very low temperatures ($< 1300K$), the dissipation is lower compared to those with intermediate temperatures ($1300 - 1600K$). The latter is due to the mixing between burning and very low temperature samples; therefore, the mixture fraction was well mixed but temperature was not.

- For large SGS variance, the dissipation indicates strained or extinguished laminar flamelets; however, the pilot flame played an important role. For samples not far from equilibrium, the dissipation is consistent with strained laminar flamelets. Further away from equilibrium, there are dissipation peaks at intermediate temperature (as high as 1700K), which are probably a result of the rapid mixing between the pilot gas and the lean or rich mixtures, corresponding to extinguished flamelets.

- The conditional-sampling-based noise and resolution corrections for scalar dissipation rate measurements can guarantee selection of well-resolved local scalar fields to accurately determine the noise variance and remove the noise contribution. The conditional sampling procedure, combined with the ramp-cliff model, enables accurate determination of the dissipation length scale and correction for under-resolution.

In collaboration with Professors Pope and Givi we currently are working on testing models and LES predictions (FMDF, etc.) and are exploring the possibilities of using the above results to improve models. In particular, the issue of the ability of mixing models to predict the very different SGS mixing characteristics of conserved scalars (mixture fraction) and reactive scalars (temperature) will be explored.

## References


[1] S. B. Pope, "Computations of turbulent combustion: Progress and challenges," in *Proceedings of the 23rd Symposium (International) on Combustion* (1990), pp. 591–612.

[2] L. Y. M. Gicquel, P. Givi, F. A. Jaberi, and S. B. Pope, "Velocity filtered density function for large eddy simulation of turbulent flows," Phys. Fluids **14,** 1196–1213 (2002).

[3] M. R. H. Sheikhi, T. G. Drozda, P. Givi, and S. B. Pope, "Velocity-scalar filtered density function for large eddy simulation of turbulent flows," Phys. Fluids **15,** 2321–2337 (2003).

[4] R. S. Barlow and A. N. Karpetis, "Measurements of scalar variance, scalar dissipation, and length scales in turbulent piloted methane/air jet flames," Flow, Turb. Combust. **72,** 427–448 (2004).

[5] A. N. Karpetis and R. S. Barlow, "Measurements of flame orientation and scalar dissipation in turbulent partially premixed methane flames," Proc. Combust. Inst. **30,** 665–672 (2005).

[6] R. S. Barlow and A. N. Karpetis, "Scalar length scales and spatial averaging effects in turbulent piloted methane/air jet flames," Proc. Combust. Inst. **30,** 673–680 (2005).

[7] R. Bilger, S. Starner, and R. Kee, "On reduced mechanisms for methane-air combustion in nonpremixed flames," Combust. Flame **80,** 135–149 (1990).

[8] J. Cai, D. Wang, C. Tong, R. S. Barlow, and A. N. Karpetis, "Investigation of subgrid-scale mixing of mixture fraction and temperature in turbulent partially premixed flames," Proc. Combust. Inst. **32,** 1517–1525 (2009).

[9] J. Cai, R. S. Barlow, A. N. Karpetis, and C. Tong, "Conditionally filtered diffusion of mixture fraction and temperature in turbulent partially premixed flames," Proc. Combust. Inst. **33,** 1505–1513 (2011).

[10] C. Tong, "Measurements of conserved scalar filtered density function in a turbulent jet," Phys. Fluids **13,** 2923–2937 (2001).

[11] D. Wang and C. Tong, "Conditionally filtered scalar dissipation, scalar diffusion, and velocity in a turbulent jet," Phys. Fluids **14,** 2170–2185 (2002).

[12] D. Wang and C. Tong, "Experimental study of velocity-scalar filtered joint density function for LES of turbulent combustion," Proc. Combust. Inst. **30,** 567–574 (2005).

[13] A. N. Kolmogorov, "A refinement of previous hypothesis concerning the local structure of turbulence in a viscous incompressible fluid at high Reynolds number," J. Fluid Mech. **13,** 82–85 (1962).

[14] A. G. Rajagopalan and C. Tong, "Experimental investigation of scalar-scalar-dissipation filtered joint density function and its transport equation," Phys. Fluids **15,** 227–244 (2003).

[15] D. Wang, C. Tong, and S. B. Pope, "Experimental study of velocity filtered joint density function and its transport equation," Phys. Fluids **16,** 3599–3613 (2004).

[16] D. Wang, C. Tong, R. S. Barlow, and A. N. Karpetis, "Experimental study of scalar filtered mass density function in turbulent partially premixed flames," Proc. Combust. Inst. **31,** 1533–1541 (2007).

[17] C. Tong and Z. Warhaft, "On passive scalar derivative statistics in grid turbulence," Phys. Fluids **6,** 2165–2176 (1994).

## Publications resulted from this research


1. Cai, J., Wang, D., Tong, C., Barlow, R.S., and Karpetis, A.N. 2009 Investigation of subgrid-scale mixing of mixture fraction and temperature in turbulent partially premixed flames. *Proc. Combust. Inst.* **32**, 1517–1525.

2. Cai, J. and Tong, C. 2009 A conditional-sampling-based method for noise and resolution corrections for scalar dissipation rate measurements. *Phys. Fluids* **21**, 065104.

3. Cai, J., Barlow, R.S., and Karpetis, and Tong, C. 2010 Noise correction and length scale estimation for scalar dissipation rate measurements in turbulent partially premixed flames. *Flow Turb. Combust.* **85**, 309–332.

4. Cai, J., Barlow, R.S., and Karpetis, and Tong, C. 2011 Conditionally filtered diffusion of mixture fraction and temperature in turbulent partially premixed flames. *Proc. Combust. Inst.* **33**, 1505–1513.

5. Cai, J. and Tong, C. 2012 Investigation of subgrid-scale mixing of mixture fraction, temperature and species mass fractions in turbulent partially premixed flames. *Proc. Combust. Inst.* **34**, In press.

**Presentations on the results from this research**

1. Investigation of subgrid-scale mixing of mixture fraction, temperature and species mass fractions in turbulent partially premixed flames. The thirty fourth International Symposium on Combustion. Warsaw, 2012

2. A conditional-sampling-based method for noise and resolution corrections for scalar dissipation rate measurements. 64th Annual Meeting of the Division of Fluid Dynamics of the American Physical Society. Los Angeles 2011.

3. Species filtered mass density function and conditionally filtered dissipation rate in turbulent partially premixed flames. 7th US national Meeting on Combustion. Atlanta, 2011

4. Conditionally filtered diffusion of mixture fraction and temperature in turbulent partially premixed flames. The thirty third International Symposium on Combustion. Beijing, 2010

5. Investigation of subgrid-scale mixing and turbulence-chemistry interaction in turbulent partially premixed flames using experimental data. Institute of Combustion Technology. University of Aachen, Germany. 2010 (**Invited talk**)

6. Conditionally filtered diffusion of mixture fraction and temperature in turbulent partially premixed flames. 6th US national Meeting on Combustion. Ann Arbor, 2009

## Participating Personnel

Chenning Tong: Professor (12/01/2008-11/30/2011)

Jian Cai: Graduate student (12/01/2008-07/30/2010)

Shuaishuai Liu: Graduate student (08/01/2010-11/30/2011)

### Interactions with researchers at AFRL

During the period of this grant, The PI continued the collaboration with Dr. Campbell Carter. In 2004 the PI initiated contacts with several researchers at AFRL to seek opportunities for collaborations. The discussions with Dr. Carter resulted in a collaborative project. In the summers of 2005 and 2006 the PI spent several weeks at AFRL as part of the collaboration.

This collaboration focuses primarily on issues of using measurements to improve of large eddy simulation (LES) of nonpremixed turbulent combustion. In PDF-based LES approaches the subgrid-scale mixing of multiple scalars must be modeled. Current mixing models are based primarily on knowledge gained from two-stream mixing problems (e.g., fuel mixing with oxidizer); however, in a reacting flow at least three scalars are involved (the third is a product). Understanding of three-stream SGS mixing, therefore, is important for modeling mixing in nonpremixed turbulent combustion. As a step toward understanding SGS mixing of multiple reactive scalars, the PI and Dr. Carter are studying the SGS mixing in a three-stream non-reacting jet. The jet nozzle consists of an axisymmetric jet and an annulus from which acetone-doped air and ethylene are issued into an air co-flow. Laser diagnostics (planar laser induced fluorescence and Rayleigh scattering) were employed to obtain images of the species. The PI currently is analyzing the data. This study will provide a basis for future investigations of multi-scalar SGS mixing in turbulent flames.

## Inventions

None